AD-A124 664 ANALYTICAL/EXPERIMENTAL LINEAR BIFURCATION OF CURVED CYLINDRICAL COMPOSITE PANELS(U) AIR FORCE INST OF TECH WRIGHT-PATTERSON AFB OH SCHOOL OF ENGI.. J S HEBERT 1/2

UNCLASSIFIED DEC 82 AFIT/GAE/AA/82D-14 F/G 13/13 NL

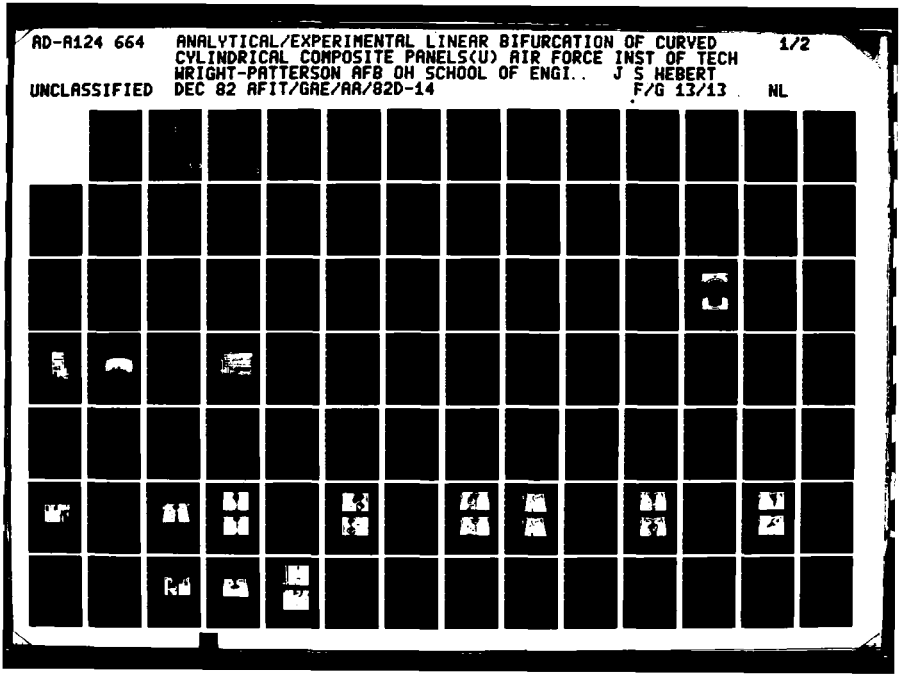

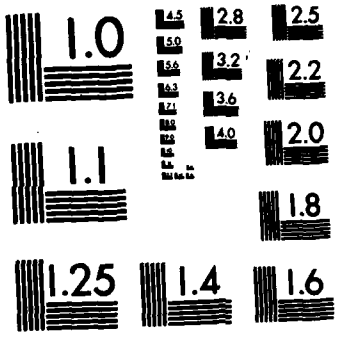

(1)

AIR FORCE INSTITUTE OF TECHNOLOGY

AIR UNIVERSITY
UNITED STATES AIR FORCE

ANALYTICAL/EXPERIMENTAL LINEAR BIFURCATION
OF CURVED CYLINDRICAL COMPOSITE PANELS

THESIS

John S. Hebert
Capt USAF

AFIT/GAE/AA/82D-14

SCHOOL OF ENGINEERING

WRIGHT-PATTERSON AIR FORCE BASE, OHIO

AFIT/GAE/AA/82D-14

ANALYTICAL/EXPERIMENTAL LINEAR BIFURCATION OF CURVED CYLINDRICAL COMPOSITE PANELS

THESIS

John S. Hebert

AFIT/GAE/AA/82D-14 Capt USAF

AFIT/GAE/AA/82D-14

ANALYTICAL/EXPERIMENTAL LINEAR BIFURCATION OF CURVED CYLINDRICAL COMPOSITE PANELS

THESIS

Presented to the Faculty of the School of Engineering

of the Air Force Institute of Technology

Air University (ATC)

in Partial Fulfillment of the

Requirements for the Degree of

Master of Science

by

John S. Hebert

Capt USAF

Graduate Aeronautical Engineering

December 1982

Acknowledgements

I wish to express my extreme gratitude to Dr. Anthony Palazotto for his patience and expert guidance throughout this thesis.

I would also like to thank the Air Force Flight Dynamics Laboratory, in particular Dr. N.S. Khot and Capt Marvin Becker, for the support and funding that was necessary to conduct this analysis.

Many thanks to Capt Thomas Janisse for his help with the STAGSC-1 Computer Code.

To my wife, Rhonda, and sons, Matthew and Todd, thank you for all the support you gave me when I needed it the most.

Contents

Contents (Cont'd.)

List of Symbols

A_{ij}	Extensional Stiffnesses
B_{ij}	Coupling Stiffnesses
C	Panel Chord Length
D_{ij}	Bending Stiffnesses
E_1	Longitudinal Modulus of Elasticity
E_2	Transverse Modulus of Elasticity
G	Shear Modulus
L	Panel Length
M_x, M_y, M_{xy}	Moment Resultants
N_x, N_y, N_{xy}	Force Resultants
Q_{ij}	Reduce Stiffnesses
$\bar{Q}_{ij}$	Transformed Reduced Stiffnesses
r,R	Panel Radius
t	Panel Thickness
u,v,w	Displacements in the x,y,z Directions, Respectively
x,y,z	Structural Coordinate Directions
1,2,3	Lamina Principal Axis Directions
γ	Shear Strain
θ	Ply Orientation

List of Symbols (Cont'd.)

κ	Curvature
ν	Poisson's Ratio
σ	Normal Stress
τ	Shearing Stress
$w_{,x}$	Comma Denotes Partial Difference
ε°	Zero Superscript Denotes a Middle Surface Value
ϕ	Rotation of a Tangent to the Panel's Middle Surface
Z	Distance From a Panel's Middle Surface

List of Figures

List of Figures (Cont'd.)

List of Figures (Cont'd.)

List of Tables

Abstract

The buckling loads of 8-ply unstiffened laminated (graphite-epoxy) cylindrical panels were determined experimentally. The results were compared to the linear bifurcation loads as determined by the STAGSC-1 Computer Code. The analysis included three different ply orientations, five different aspect ratios (length÷chord), and one set of boundary conditions; clamped along the top and bottom curved edges and simply supported along the vertical sides. The experimental tests were conducted by the Air Force Flight Dynamics Laboratory using a redesigned test set-up. Fairly good agreement was obtained between the analytical and experimental loads, with the linear bifurcation values being 3% to 32% higher than the experimental. It was evident that the buckling pattern observed experimentally did not in all cases correspond to the symmetrical pattern generated by STAGSC-1. This was due mainly to the test fixtures inability to evenly distribute the stress along the simple support mechanism.

ANALYTICAL/EXPERIMENTAL LINEAR BIFURCATION OF CURVED CYLINDRICAL COMPOSITE PANELS

I. INTRODUCTION

Background

Composite materials' high strength to weight ratio make it particularly well suited for aircraft structural use. The USAF's forward swept aircraft design [1] is an excellent example of the materials' advantage in that through proper composite "tailoring", the problem of aeroelastic divergence can be practically avoided without the enormous weight gain associated with conventional metals. However, in comparison with metals the science of composites is still in its infancy, therefore, engineers are reluctant to base their design solely on computer generated data without some comparison to realistic emperical data.

Numerous articles have dealt with the analysis of composite cylinders and flat plates [2-4]. But due to manufacturing difficulties and the lack of experimental test fixtures, literature on actual experimentation of cylindrical composite panels is relatively scarce. One of the first and most influential articles on the subject was presented by Wilkens [5] in 1974. Using a unique test set-up, he determined the buckling loads of different ply orientations associated with one width to length ratio (referred to as the aspect ratio). His results show percent knockdown factors $\left(\left(1 - \frac{\text{experimental buckling load}}{\text{theoretical buckling load}}\right) \times 100\right)$ ranging from 1% to 66%. He also found that multidirectional laminates

retain a high percentage of their buckling strength after repeated buckling. More recently, Bauld [6] used a modification of Wilkens' test fixture to study the experimental buckling loads of composite cylindrical panels having two different ply orientations and five different aspect ratios. In particular, he found that circumferential imperfections in a panel serve to lower its resistance to buckling. This thesis is a continuation of the work done by Becker [7], with a redesigned experimental test fixture which allows an even distribution of applied load and thus a more reliable set of experimental results. The work reported herein involved a new set of aspect ratios allowing for a broader appreciation of panel buckling.

Purpose

The purpose of this thesis is to compare experimentally determined buckling loads of cylindrical composite panels to the linear bifurcation loads calculated by the STAGSC-1 Computer Code. The effect of ply orientation and aspect ratio will be the two major variables. The results will be used to further the understanding of composite buckling behavior when subjected to design loads [8].

Scope

A total of 30 panels were tested and aspect ratios of $\frac{1}{2}$ (8"x16"), $\frac{3}{4}$ (12"x16"), 1 (16"x16"), $\frac{4}{3}$ (16"x12"), and 2 (16"x8") were physically included. All panels consisted of 8-ply graphite-epoxy with experimentally determined material properties of [7]:

$$E_1 = 20.5 \times 10^6$$

$$E_2 = 1.3 \times 10^6$$

$$G_{12} = 0.75 \times 10^6$$

$$\nu_{12} = 0.335$$

The three different ply orientations used are $(\pm 45)_{2s}$, $(90,0)_{2s}$, and $(90,\pm 45,0)_s$. Figure 1 shows a typical panel and defines the panel notations and sign conventions. The panel boundary conditions incorporated in this work consists of a clamped top curved edge (u=free, $v=w=w_{,x}=0$), a clamped bottom curved edge ($u=v=w=w_{,x}=0$), and simple supports along the vertical sides ($u=v=w_{,y}$=free,w=0). See Fig. 1 for positive displacement directions. It should be noted that the 30 panels represent a duplication of each unique ply orientation and aspect ratio, thus an average experimental buckling load can be obtained for a given set of parameters.

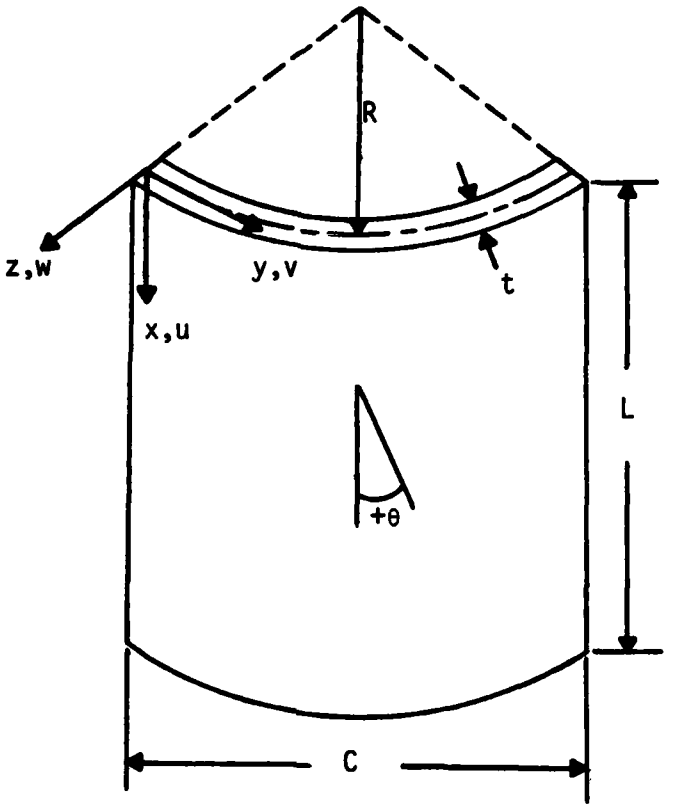

t = thickness = 8 plies @ 0.005" = 0.04"

R = radius = 12"

C = chord length

L = length

x,y,z = structural coordinate directions

θ = ply orientation

u,v,w = displacements

L/C = aspect ratio

Figure 1 Panel Notation

II. THEORY

Bifurcation Buckling

Bifurcation involves the transfer of membrane strain energy to bending strain energy. Bushnell [9] has shown that a thin shell (cylindrical panel in this thesis) can absorb a great deal of membrane strain energy with little deformation. The shell must deform much more for it to absorb an equivalent amount of bending strain energy. It is through these larger deformations that the transfer of energies will occur resulting in bifurcation.

The above explanation is best illustrated by relating it to a panel's load-displacement curve, or synonymously, its equilibrium path [10]. Figure 2 shows the load versus end displacement relationship for a thin-walled cylindrical panel subjected to axial compression. The primary equilibrium path is intersected by a secondary path which is characterized by a dramatic drop-off in load and a negative slope. The intersection is the bifurcation point and represents the buckled configuration of the panel. At bifurcation, the shell's equilibrium equations have multiple solutions. The so-called secondary path represents a stable solution while the portion of the load-displacement curve that lies above the bifurcation point, referred to as the primary path, is unstable.

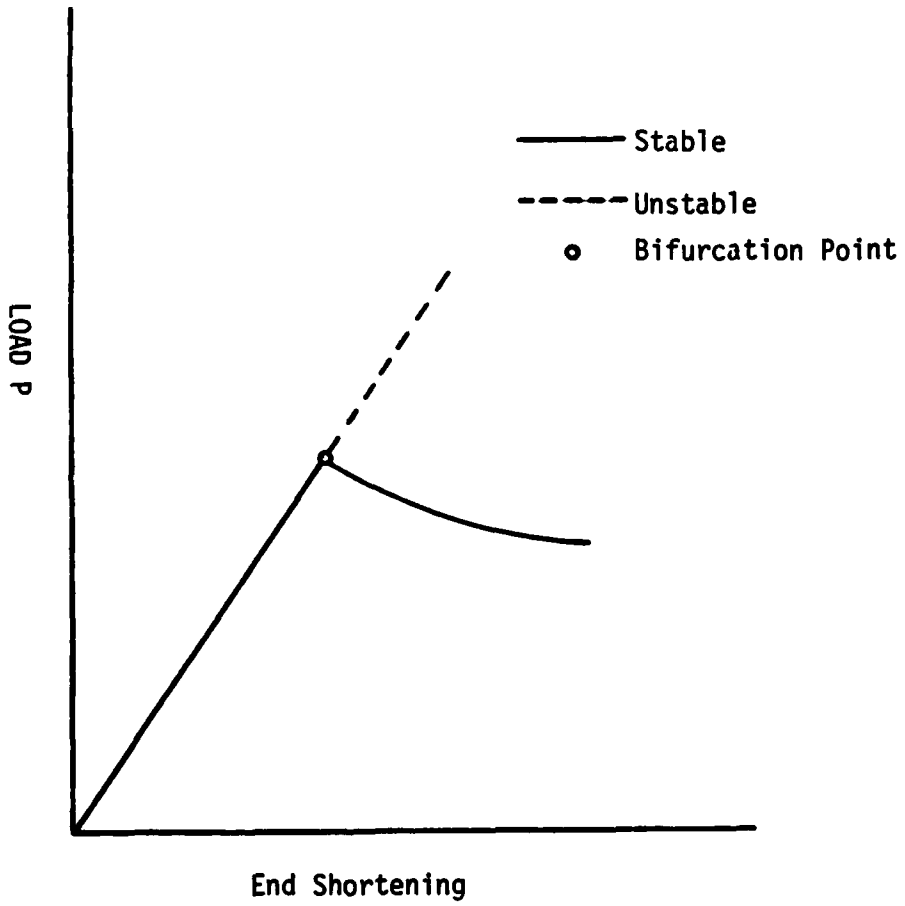

Figure 2 Load-End Displacement Curve for Bifurcation

Classical Lamination Theory

The basic constitutive relationships are essential to the understanding of composite laminae behavior. References [11] and [12] present a detailed development of these equations and should be referred to by the interested reader.

Before a complete laminate made up of N layers can be analyzed, a brief description of the stress-strain relationship for an individual laminae must be presented. The stress-strain relations in principal material coordinates (see Fig. 3) for a laminae of orthotropic material under plane stress can be written as

$$\begin{Bmatrix} \sigma_1 \\ \sigma_2 \\ \tau_{12} \end{Bmatrix} = \begin{bmatrix} Q_{11} & Q_{12} & 0 \\ Q_{12} & Q_{22} & 0 \\ 0 & 0 & Q_{66} \end{bmatrix} \begin{Bmatrix} \epsilon_1 \\ \epsilon_2 \\ \gamma_{12} \end{Bmatrix} \tag{1}$$

where Q_{ij} is the reduced stiffnesses and are defined in terms of engineering constants

$$\begin{aligned} Q_{11} &= E_1/(1-\nu_{12}\nu_{21}) \\ Q_{12} &= \nu_{12}E_2/(1-\nu_{12}\nu_{21}) = \nu_{21}E_1/(1-\nu_{12}\nu_{21}) \\ Q_{22} &= E_2/(1-\nu_{12}\nu_{21}) \\ Q_{66} &= G_{12} \end{aligned} \tag{2}$$

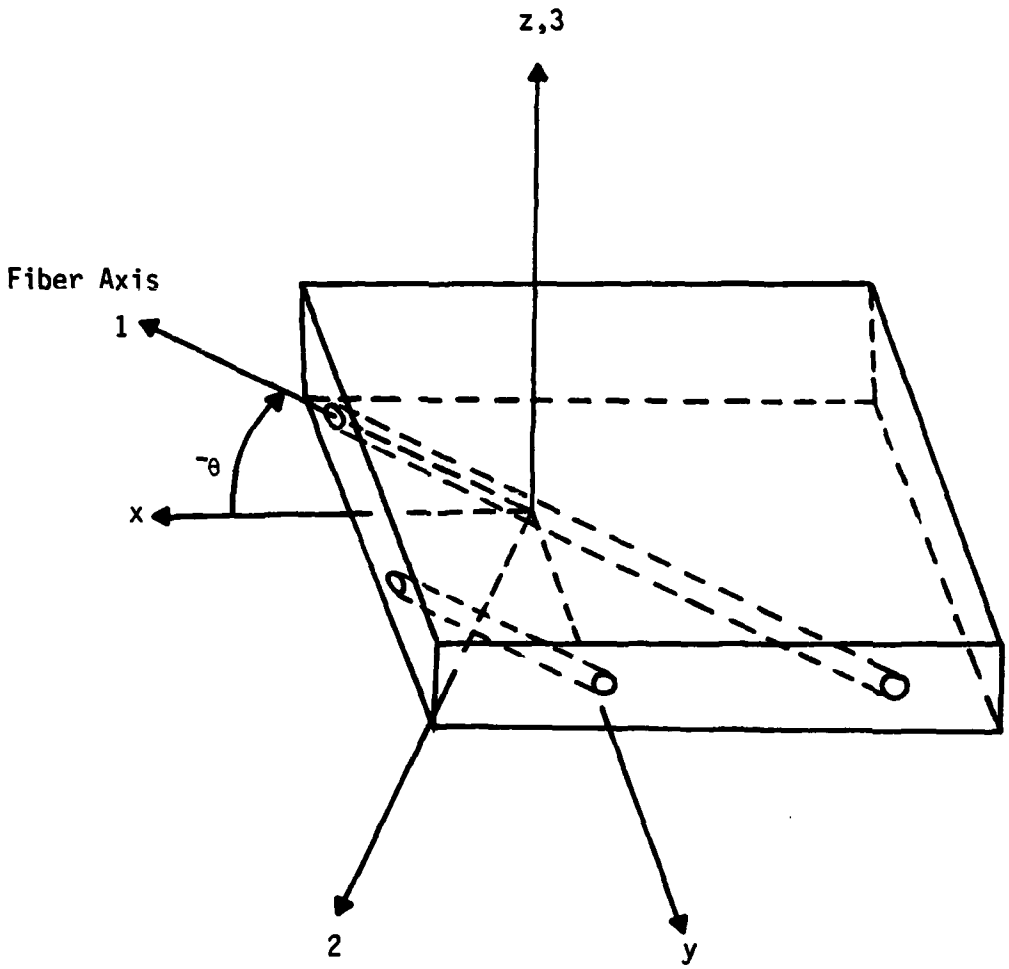

x,y,z = Structural Axes

1,2,3 = Lamina Principal Axes

Figure 3 Definition of Coordinate Systems [7]

where

$$\nu_{12} = -\frac{\varepsilon_2}{\varepsilon_1}$$

$$\nu_{21} = -\frac{\varepsilon_1}{\varepsilon_2} \tag{3}$$

$$G_{12} = -\frac{\tau_{12}}{\gamma_{12}}$$

In any other coordinate system with the fiber axis oriented at some angle, θ, with respect to the structural axes, the stresses are

$$\begin{Bmatrix} \sigma_x \\ \sigma_y \\ \tau_{xy} \end{Bmatrix} = \begin{bmatrix} \bar{Q}_{11} & \bar{Q}_{12} & \bar{Q}_{16} \\ \bar{Q}_{12} & \bar{Q}_{22} & \bar{Q}_{26} \\ \bar{Q}_{16} & \bar{Q}_{26} & \bar{Q}_{66} \end{bmatrix} \begin{Bmatrix} \varepsilon_x \\ \varepsilon_y \\ \gamma_{xy} \end{Bmatrix} \tag{4}$$

where $\bar{Q}_{ij}$ are the transformed reduced stiffness

$$\begin{aligned}
\bar{Q}_{11} &= Q_{11}\cos^4\theta + 2(Q_{12} + 2Q_{66})\sin^2\theta\cos^2\theta + Q_{22}\sin^4\theta \\
\bar{Q}_{12} &= (Q_{11} + Q_{22} - 4Q_{66})\sin^2\theta\cos^2\theta + Q_{12}(\sin^4\theta + \cos^4\theta) \\
\bar{Q}_{22} &= Q_{11}\sin^4\theta + 2(Q_{12} + 2Q_{66})\sin^2\theta\cos^2\theta + Q_{22}\cos^4\theta \\
\bar{Q}_{16} &= (Q_{11} - Q_{12} - 2Q_{66})\sin\theta\cos^3\theta + (Q_{12} - Q_{22} + 2Q_{66}) \\
&\quad \sin^3\theta\cos\theta \\
\bar{Q}_{26} &= (Q_{11} - Q_{12} - 2Q_{66})\sin^3\theta\cos\theta + (Q_{12} - Q_{22} + 2Q_{66}) \\
&\quad \sin\theta\cos^3\theta \\
\bar{Q}_{66} &= (Q_{11} + Q_{22} - 2Q_{12} - 2Q_{66})\sin^2\theta\cos^2\theta + Q_{66}(\sin^4\theta + \cos^4\theta)
\end{aligned} \tag{5}$$

Equation (4) can be thought of as the stress-strain relations for the K^{th} Layer of a multilayered laminate. Thus, it can be written as

$$\{\sigma\}_k = [\bar{Q}]_k \{\varepsilon\}_k \tag{6}$$

To expand the discussion to a multilayered laminate, a few assumptions must be made. First, the laminate is presumed to consist of perfectly bonded laminae so that no lamina can slip relative to another. Secondly, adherence to the Kirchhoff-Love hypothesis dictates that sections normal to the panel's mid-surface remain plane and normal to that surface after bending [11]. These assumptions lead to the following strain-curvature relationship for a laminate

$$\begin{Bmatrix} \varepsilon_x \\ \varepsilon_y \\ \gamma_{xy} \end{Bmatrix} = \begin{Bmatrix} \varepsilon_x^0 \\ \varepsilon_y^0 \\ \gamma_{xy}^0 \end{Bmatrix} + Z \begin{Bmatrix} \kappa_x \\ \kappa_y \\ 2\kappa_{xy} \end{Bmatrix} \tag{7}$$

where the o superscript indicates the mid-surface strains, the κ's are mid-surface curvatures and Z represents a distance from the panel mid-surface. For a cylindrical panel with moderately large displacements and also moderately large rotations of tangents to its mid-surface, the above strains and curvatures are given by Sanders' kinematic relations without initial imperfections [13]

$$\varepsilon_x^0 = u_{,x} + \frac{1}{2}\phi_x^2 + \frac{1}{2}\phi^2$$

$$\varepsilon_y^0 = v_{,x} + \frac{w}{r} + \frac{1}{2}\phi_y^2 - \frac{1}{2}\phi^2$$

$$\gamma_{xy}^0 = v_{,x} + u_{,y} + \phi_x\,\phi_y \tag{8}$$

$$\kappa_x = \phi_{x,x}$$

$$\kappa_y = \phi_{y,y}$$

$$2\kappa_{xy} = \phi_{y,x} + \phi_{x,y} + \frac{\phi}{r}$$

where u,v,w denote the axial, circumferential, and radial components of displacement, respectively, of the panel's mid-surface. The ϕ's are rotation components and are expressed in terms of the displacements as

$$\phi_x = -w_{,x}$$

$$\phi_y = -w_{,y} + \frac{v}{r} \tag{9}$$

$$\phi = \frac{1}{2}(v_{,x} - u_{,y})$$

where r is the panel's radius of curvature.

Substituting Eq. (7) into Eq. (4), the stresses in the K^{th} Layer can be expressed in terms of the laminate middle surface strains and curvatures as

$$\begin{Bmatrix}\sigma_x\\ \sigma_y\\ \tau_{xy}\end{Bmatrix}_k = \begin{bmatrix}\bar{Q}_{11} & \bar{Q}_{12} & \bar{Q}_{16}\\ \bar{Q}_{12} & \bar{Q}_{22} & \bar{Q}_{26}\\ \bar{Q}_{16} & \bar{Q}_{26} & \bar{Q}_{66}\end{bmatrix}_k \left\{ \begin{Bmatrix}\varepsilon_x^0\\ \varepsilon_y^0\\ \gamma_{xy}^0\end{Bmatrix} + Z \begin{Bmatrix}\kappa_x\\ \kappa_y\\ 2\kappa_{xy}\end{Bmatrix} \right\} \tag{10}$$

Now that the stresses in each layer are known, the resultant forces and moments acting on a laminate are obtained by integration of the stresses in each lamina through the laminate thickness. For example,

$$N_x = \int_{-t/2}^{t/2} \sigma_x dZ \tag{11}$$

and

$$M_x = \int_{-t/2}^{t/2} \sigma_x Z dZ \tag{12}$$

N_x and M_x is a force and moment per unit length (width) of the cross-section of the laminate as shown in Fig. 4, and are defined as

$$\begin{Bmatrix} N_x \\ N_y \\ N_{xy} \end{Bmatrix} = \int_{-t/2}^{t/2} \begin{Bmatrix} \sigma_x \\ \sigma_y \\ \sigma_{xy} \end{Bmatrix}_k dZ = \sum_{n=1}^{N} \int_{Z_{k-1}}^{Z_k} \begin{Bmatrix} \sigma_x \\ \sigma_y \\ \tau_{xy} \end{Bmatrix}_k dZ \tag{13}$$

and

$$\begin{Bmatrix} M_x \\ M_y \\ M_{xy} \end{Bmatrix} = \int_{-t/2}^{t/2} \begin{Bmatrix} \sigma_x \\ \sigma_y \\ \sigma_{xy} \end{Bmatrix}_k Zdz = \sum_{k=1}^{N} \int_{Z_{k-1}}^{Z_k} \begin{Bmatrix} \sigma_x \\ \sigma_y \\ \sigma_{xy} \end{Bmatrix}_k Zdz \tag{14}$$

where N is the total number of lamina, and Z_k and Z_{k-1} are defined in Fig. 5.

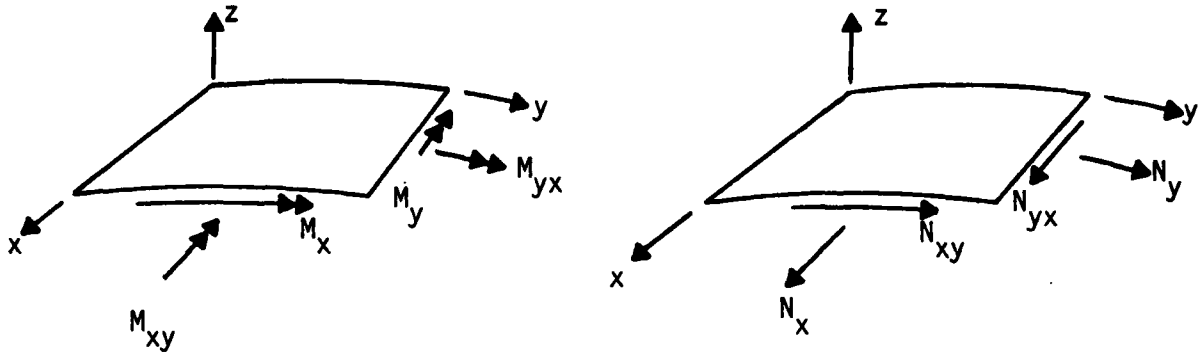

Figure 4 Forces and Moments on a Laminate

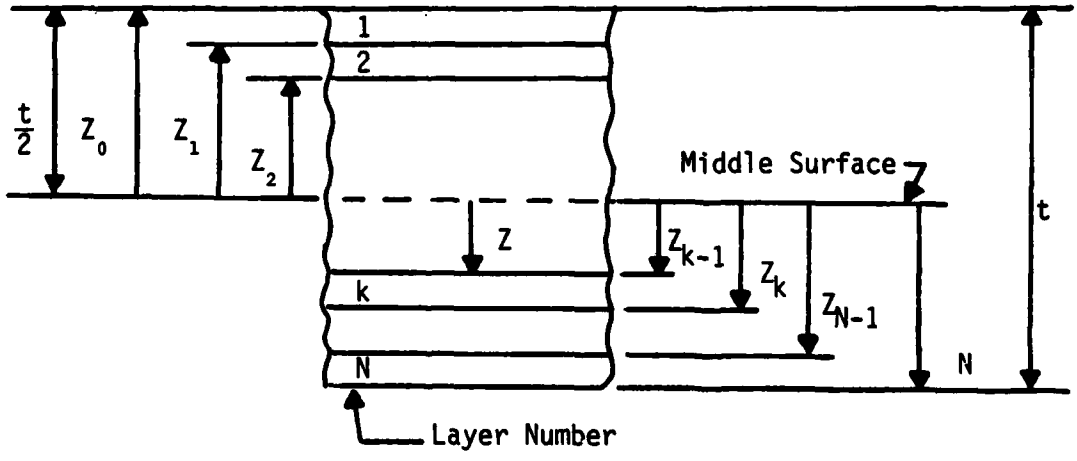

Figure 5 Geometry of an N-Layered Laminate

The integration indicated by Eq's. (13) and (14) can be rearranged to take advantage of the fact that the stiffnesses matrix, $\bar{Q}_{ij}$, for each layer is constant within that layer. Thus, the stiffness matrix goes outside the integration over each layer but is within the summation of force and moment resultants for each layer. Also, recall that ε_x^0, ε_y^0, γ_{xy}^0, κ_x, κ_y, and κ_{xy} are not functions of Z but are middle surface values so they too can be removed from under the summation signs. Thus, the force and moment equations become

$$\begin{Bmatrix} N_x \\ N_y \\ N_{xy} \end{Bmatrix} = \begin{bmatrix} A_{11} & A_{12} & A_{16} \\ A_{12} & A_{22} & A_{26} \\ A_{16} & A_{26} & A_{66} \end{bmatrix} \begin{Bmatrix} \varepsilon_x^0 \\ \varepsilon_y^0 \\ \gamma_{xy}^0 \end{Bmatrix} + \begin{bmatrix} B_{11} & B_{12} & B_{16} \\ B_{12} & B_{22} & B_{26} \\ B_{16} & B_{26} & B_{66} \end{bmatrix} \begin{Bmatrix} \kappa_x \\ \kappa_y \\ 2\kappa_{xy} \end{Bmatrix} \tag{15}$$

$$\begin{Bmatrix} M_x \\ M_y \\ M_{xy} \end{Bmatrix} = \begin{bmatrix} B_{11} & B_{12} & B_{16} \\ B_{12} & B_{22} & B_{26} \\ B_{16} & B_{26} & B_{66} \end{bmatrix} \begin{Bmatrix} \varepsilon_x^0 \\ \varepsilon_y^0 \\ \gamma_{xy}^0 \end{Bmatrix} + \begin{bmatrix} D_{11} & D_{12} & D_{22} \\ D_{12} & D_{22} & D_{26} \\ D_{16} & D_{26} & D_{66} \end{bmatrix} \begin{Bmatrix} \kappa_x \\ \kappa_y \\ 2\kappa_{xy} \end{Bmatrix} \tag{16}$$

or

$$\begin{Bmatrix} N_x \\ N_y \\ N_{xy} \\ M_x \\ M_y \\ M_{xy} \end{Bmatrix} = \left[\begin{array}{cc} [A] & [B] \\ [B] & [D] \end{array}\right] \begin{Bmatrix} \varepsilon_x^0 \\ \varepsilon_y^0 \\ \gamma_{xy}^0 \\ \kappa_x \\ \kappa_y \\ \kappa_{xy} \end{Bmatrix} \tag{17}$$

where

$$A_{ij} = \sum_{k=1}^{N} (\bar{Q}_{ij})_k \, (Z_k - Z_{k-1})$$

$$B_{ij} = \frac{1}{2} \sum_{k=1}^{N} (\bar{Q}_{ij})_k \, (Z_k^2 - Z_{k-1}^2) \qquad (18)$$

$$D_{ij} = \frac{1}{3} \sum_{k=1}^{N} (\bar{Q}_{ij})_k \, (Z_k^3 - Z_{k-1}^3)$$

The A_{ij} are called extensional stiffnesses, the B_{ij} are called coupling stiffnesses, and the D_{ij} are called bending stiffness. The mid-surface strains and curvatures are expressed in terms of displacements (Eq's. (8) and (9)) to yield

$$\begin{Bmatrix} \varepsilon_x^0 \\ \varepsilon_y^0 \\ \gamma_{xy}^0 \\ \kappa_x \\ \kappa_y \\ 2\kappa_{xy} \end{Bmatrix} = \begin{Bmatrix} u_{,x} + \frac{1}{2} w_{,x}^2 + \frac{1}{8} (v_{,x} - u_{,y})^2 \\ v_{,y} + \frac{w}{r} + \frac{1}{2} (-w_{,y} + \frac{v}{r})^2 - \frac{1}{8} (v_{,x} - u_{,y})^2 \\ v_{,x} + u_{,y} + w_{,x} w_{,y} - w_{,x} \frac{v}{r} \\ -w_{,xx} \\ -w_{,yy} + \frac{v_{,y}}{r} \\ -w_{,yx} + \frac{v_{,x}}{r} - w_{,xy} + \frac{1}{2} (v_{,x} - u_{,y})/r \end{Bmatrix} \qquad (19)$$

STAGSC-1 Theory

STAGSC-1 (Structural Analysis of General Shells) is a computer code developed by the Lockheed Palo Alto Research Laboratory to analyze general shells under various static, thermal, and mechanical loading [14]. The approach used by STAGSC-1 is an energy-based finite element analysis. According to the energy method, a system's total potential energy is used to derive its equilibrium equations from which stability can be determined by the solution to an eigenvalue problem.

A shell's total potential energy is equal to its internal strain energy minus the product of the external forces and their respective deflections.

An element's strain energy is given by [13]:

$$U = \frac{1}{2} \int_{\text{Area}} [\epsilon]_o^T [N] [\epsilon]_o \times \text{Area} \qquad (20)$$

where

$$[\epsilon]_o = \begin{Bmatrix} e_x^0 \\ e_y^0 \\ 2e_{xy}^0 \\ \kappa_x \\ \kappa_y \\ 2\kappa_{xy} \end{Bmatrix}$$

and

$$[N] = \begin{bmatrix} [A] & [B] \\ [B] & [D] \end{bmatrix}$$

The expressions for the mid-surface strains are given in Eq's. (19) and [N] was presented in Eq. (17). In general, the strain vector $[\epsilon]_o$ is

a function of the mid-surface displacements u,v,w, the first order derivatives of u,v,w and the second order derivatives of w. Therefore, we can let a vector [d] represent this functional dependence of $[\varepsilon]_o$ on the displacements by

$$[d]^T = [u,u_{,x},u_{,y},v,v_{,x},v_{,y},w,w_{,x},w_{,y},w_{,xx},w_{,xy},w_{,yy}] \quad (21)$$

By using vector [d], Bauld [13] carried out the integration of Eq. (20) and found that the expression for strain energy is comprised of three distinct parts. The first part is quadratic in displacements, the second part is cubic in displacements, and the third part is quartic in displacements. In a finite element analysis, vector [d] is represented by an element's shape functions and nodal degrees of freedom. Thus, the strain energy can be expressed in terms of an element's degrees of freedom. An element's external potential energy is obtained by using a similar finite element analysis on its external forces. The strain energy and external potential energy is combined to give the total system potential energy, V, and can be written in the form given by Bauld [13] as

$$V = (\tfrac{1}{2}A_{rs} + \tfrac{1}{6}N1_{rs} + \tfrac{1}{12}N2_{rs})q_r q_s - R_s q_s \quad (22)$$

A_{rs} is the system's linear stiffness matrix with no dependence on the displacement vector, q. $N1_{rs}$ and $N2_{rs}$ are matrices with linear and

quadratic dependence, respectively, on displacement. R_s is the surface force vector.

The principle of total potential energy states that the equilibrium configuration of a conservative mechanical system corresponds to a stationary value of the total potential energy of the system [15]. Therefore, taking the first variation of Eq. (22) and setting it to zero, we have a set of nonlinear, algebraic equations of the form

$$(A_{rs} + \frac{1}{2}N1_{rs} + \frac{1}{3}N2_{rs})q_s - R_r = 0 \tag{23}$$

Loss of stability (bifurcation), results when the second variation of the system's total potential energy ceases to be positive definite, or

$$\text{DET } (A_{rs} + N1_{rs} + N2_{rs}) = 0 \tag{24}$$

Equation (24) is used by STAGSC-1 to solve the eigenvalue problem of the form [10]

$$[A] + \lambda[B] + \lambda^2[C] = 0 \tag{25}$$

where [B] and [C] represent nonlinear stiffness matrices in unknown displacements and products of displacements, respectively. For a linear analysis, λ, is the proportionality constant of a convenient load level used in the equilibrium Eq's. (23) to solve for the unknown displacements. The quantities A, B, C, or equivalently, A_{rs}, $N1_{rs}$, and $N2_{rs}$ are calculated once based on the equilibrium displacements. Finally, the load proportionality parameter, λ, is incremented until a sign change on the left side of Eq. (24) occurs, signifying bifurcation.

III. FINITE ELEMENT MODELING

Boundary Conditions

The STAGSC-1 computer code has a large variety of panel boundary conditions to choose from ranging from the most rigid to the most flexible conditions that can exist in an experimental test. Reference [7] gives analytical results associated with the full range. The author's choice of a simple support along the vertical sides and clamped along the curved edges was strictly made to approximate the conditions used experimentally.

Grid Size

The determination of a finite element grid size is crucial to obtaining accurate results. Nelson [16] found that to obtain accurate results there should be at least five node points per each half sine wave of the buckled pattern in the circumferential direction. Becker [7] used this information and found that a 0.5 x 0.5 inch grid represented an ideal trade-off between accuracy and computer economics. The 0.5 x 0.5 inch grid is used in this thesis, see Fig. 6. As a means of comparison, the bifurcation load of the $(\pm 45)_{2s}$, $\frac{1}{2}$ aspect ratio panel was analytically determined by using a 1.0 x 1.0 inch grid and a 0.5 x 0.5 inch grid. The bifurcation loads differed by 15%. However, the finer grid required over six times the computer time at 10 times the cost. See Appendix B for a sample STAGSC-1 computer program.

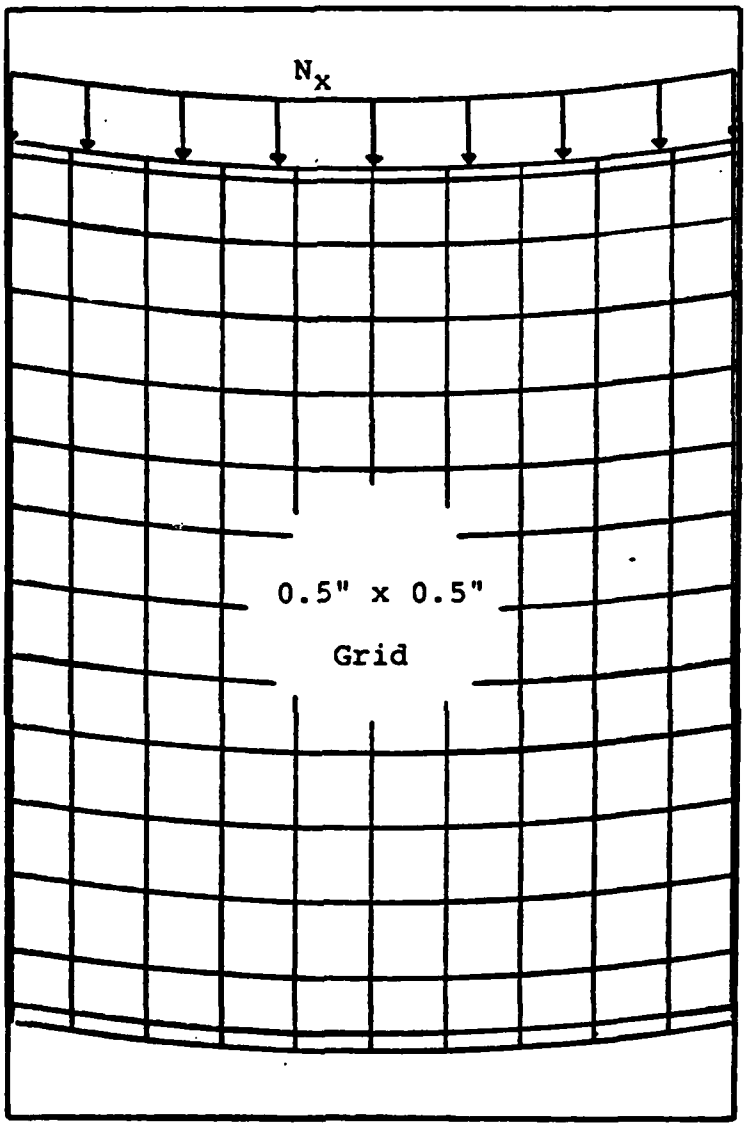

Figure 6 Finite Element Grid [7]

Finite Element Selection

Figure 7 shows the 410 Quadrilateral Plate (QUAF) element used in this thesis. The QUAF element was specifically developed to eliminate the interelement displacement incompatibility that exists when flat elements are used for curved surfaces [17]. The 410 element accomplishes this by increasing the order of the polynomial expression for the Inplane Displacement Field by virtue of a Normal Rotation Component, θ_z. The result is that each element has 6 degrees of freedom (3 translation and 3 rotation) per node for a total of 24. The 410 element works well for a linear analysis but does present problems when nonlinearity is being studied.

For nonlinear problems, the QUAF 411 element, Fig. 8, is the better choice because of the γ degrees of freedom, which represent the normal rotation of the two intersecting grid lines. A comparison of linear bifurcation loads was made using the two elements. It was found that the load varied 4% for the $(\pm 45)_{2s}$, 2-aspect ratio panel, and only .23% for the $(90,0)_{2s}$, 2-aspect ratio panel. However, the 411 element was $2\frac{1}{2}$ times more expensive. The small difference in loads correspond to the results of Snead [18] who showed that the difference in loads associated with the two elements is dependent upon panel ply orientation and the number of elements in the finite element grid. In general, the greater the number of elements, the smaller the difference.

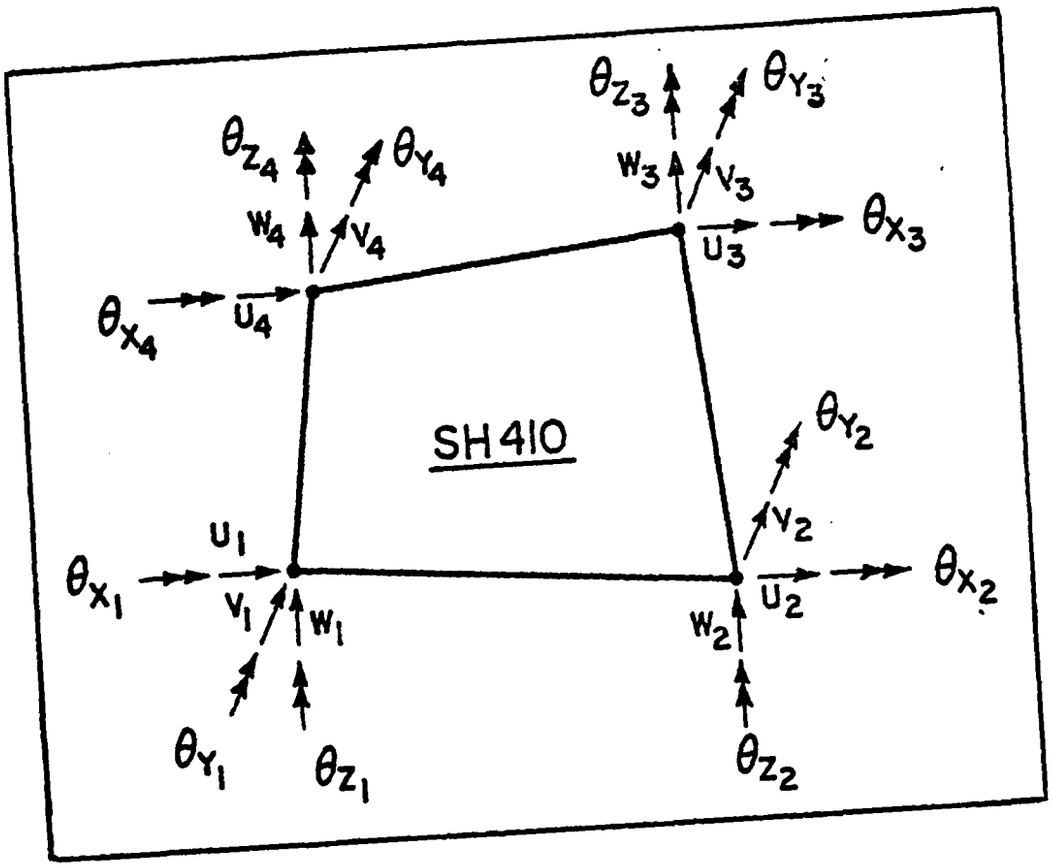

Figure 7 410 Element

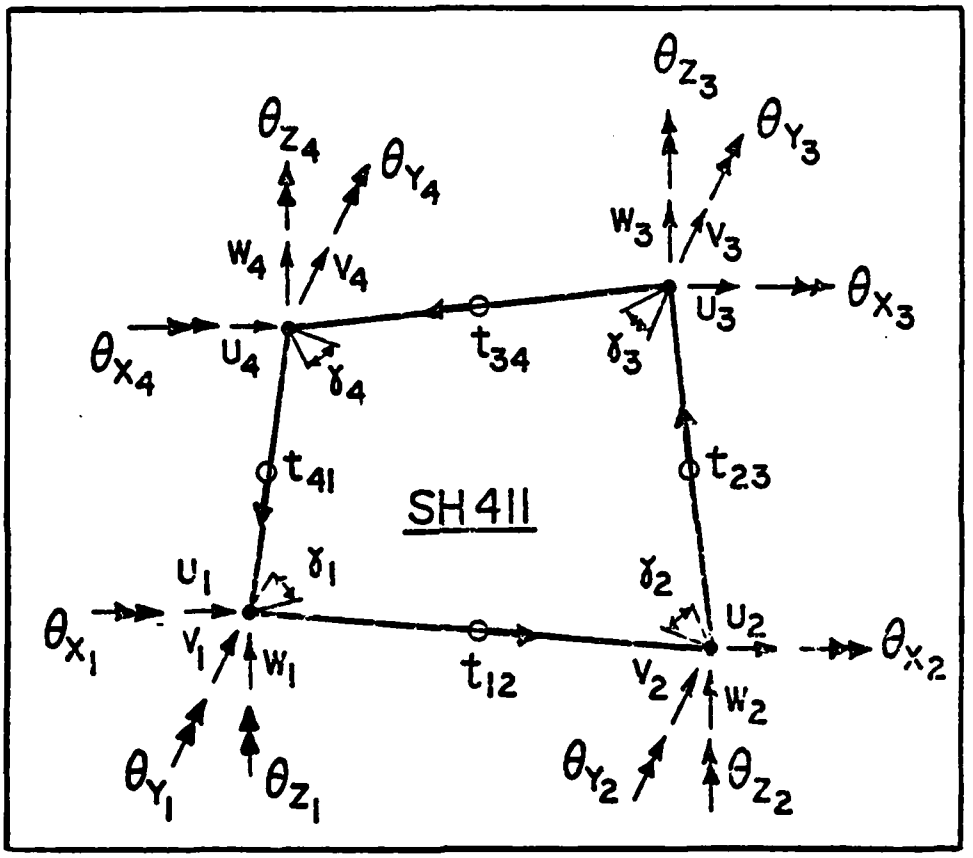

Figure 8 411 Element

IV. EXPERIMENTAL PROCEDURE

Test Panels

All of the panels tested were made from Narmco T300/5208 Graphite Epoxy and manufactured in 1979. They were originally laid up into 17" x 36" panels which were cut to the desired size by means of a specifically jigged radial arm saw with a diamond tip blade. No special techniques were used to insure "perfect" panels for the test, although every effort was made to fabricate and cut the panels as close as possible to the desired test configuration. Therefore, the normal dimensional variations (thickness, length, and width) inherent in all production processes were present [7]. Another variable that probably had some effect upon the results was the age of the panels. Although they were stored in controlled humidity and temperature conditions, these factors should be considered in critical design applications. Environmental variables are beyond the scope of this thesis.

Test Set-Up

In order to vary the boundary conditions and aspect ratios, an experimental device needed to be designed. The test fixture developed is a minor modification of the General Dynamics original 1974 design [5]. The device is shown on Fig. 9. The reader can observe the capability of this fixture to allow clamping along the panel's curved edges by virtue of the small blocks shown in Fig. 9. These blocks were forced against the panel by a series of set screws. The set screws were sufficiently

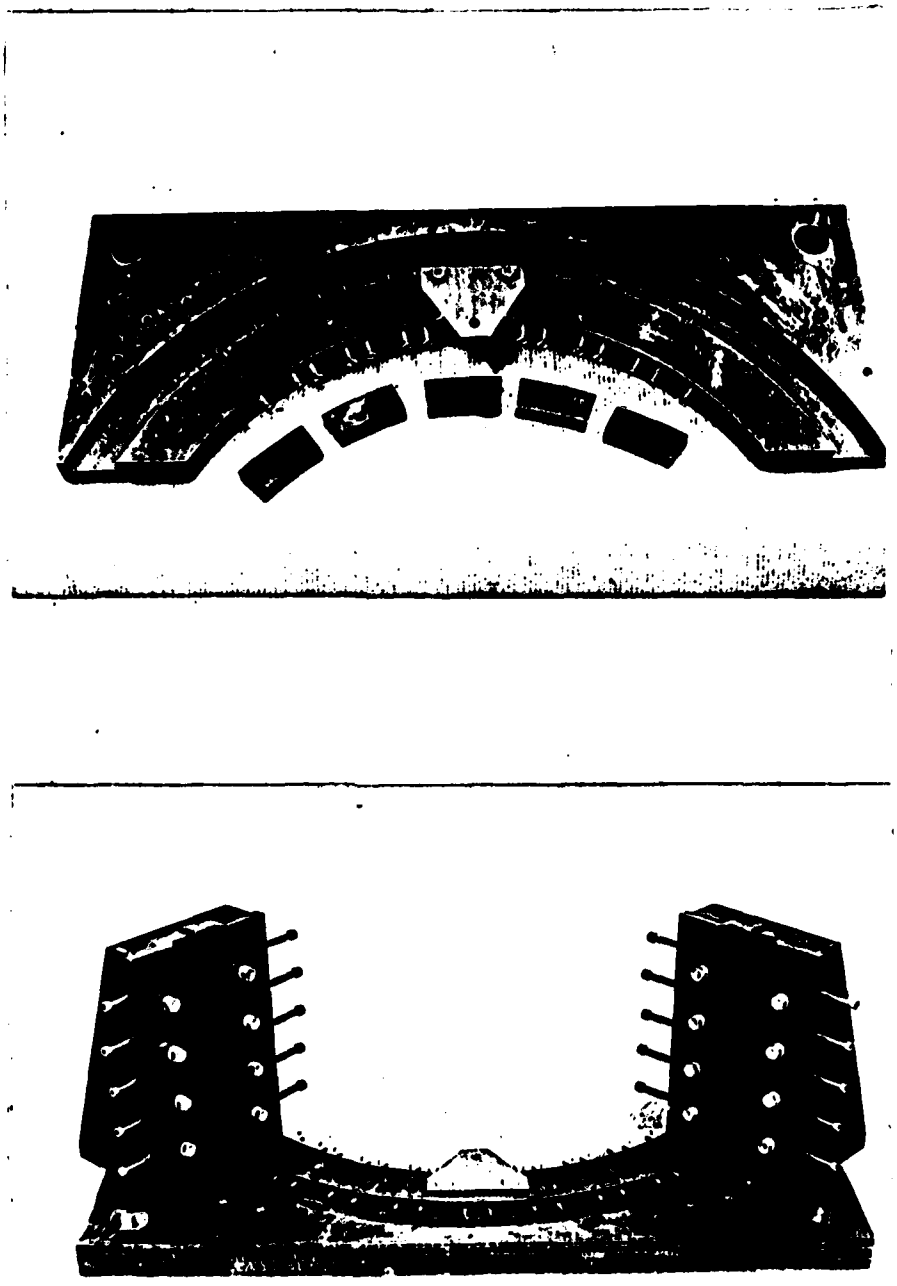

Figure 9. Panel Support Fixture

tightened by a screwdriver to insure no panel movement. The metal flange located at the center of the base plate, Fig. 9, was used to insure exact centering of the plate with respect to a duplicate top plate (for clamping along the panel's top curved edge). This technique avoids load eccentricities. A simple support condition along the panel's vertical sides is obtained by the knife-like edges shown in Fig. 9 and 10. A panel was inserted between the two knife edges and then the set screws were finger tightened until the knife edges were just touching the panel. This device prevented panel movement in the w direction but allowed movement in the u and v directions. In all tests the panels were clamped to the bottom and top plates first, then the simple supports were installed and set screws finger tightened. Figure 11 shows the complete set-up for the experimental buckling of a curved cylindrical panel. The panel support system, with panel installed, is located in the center portion of the set-up. The load is applied through a hydraulic ram to the lower steel bed which moves up the vertical sleeves of the machine. The $\frac{1}{4}$ inch panel protrusion at the top of the simple supports, see Fig. 12, allows the panel to be compressed against the top horizontal cross-head. The observed panel buckling pattern associated with the existing set-up was not symmetrical as was previously assumed. This was due to the fact that the $\frac{1}{4}$ inch panel free space was at the top of the simple supports. It was found that when the $\frac{1}{4}$ inch space was at the bottom of the support mechanism (obtained by repositioning the knife edges), the desired buckling symmetry did occur.

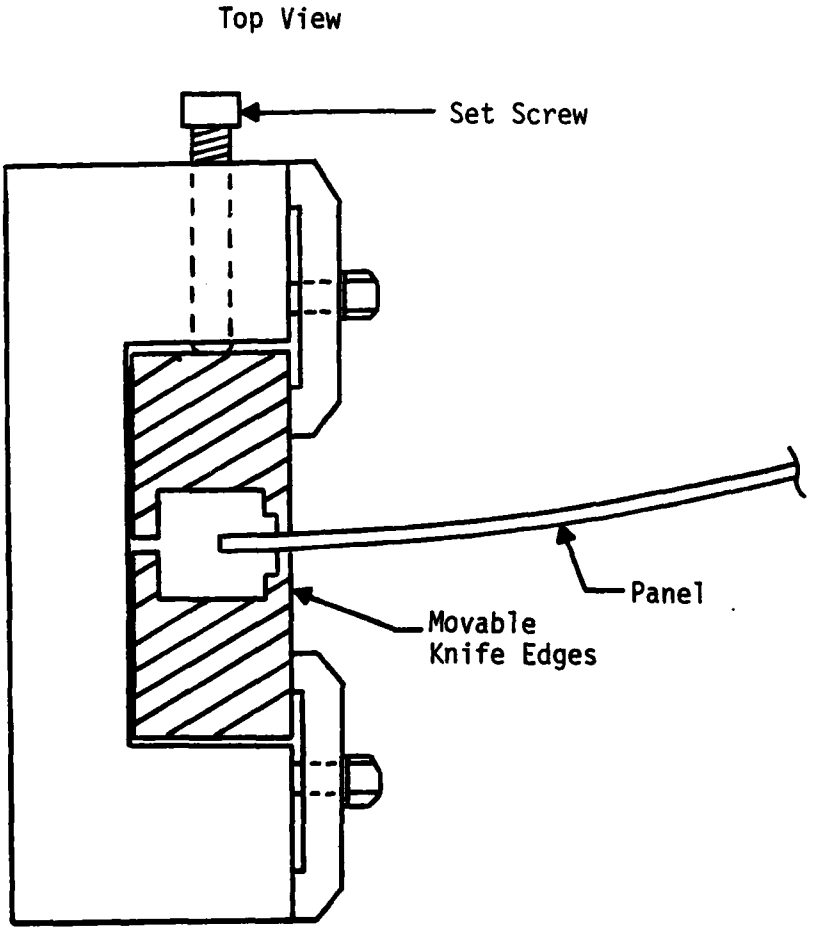

Figure 10 Simple Support Device (7)

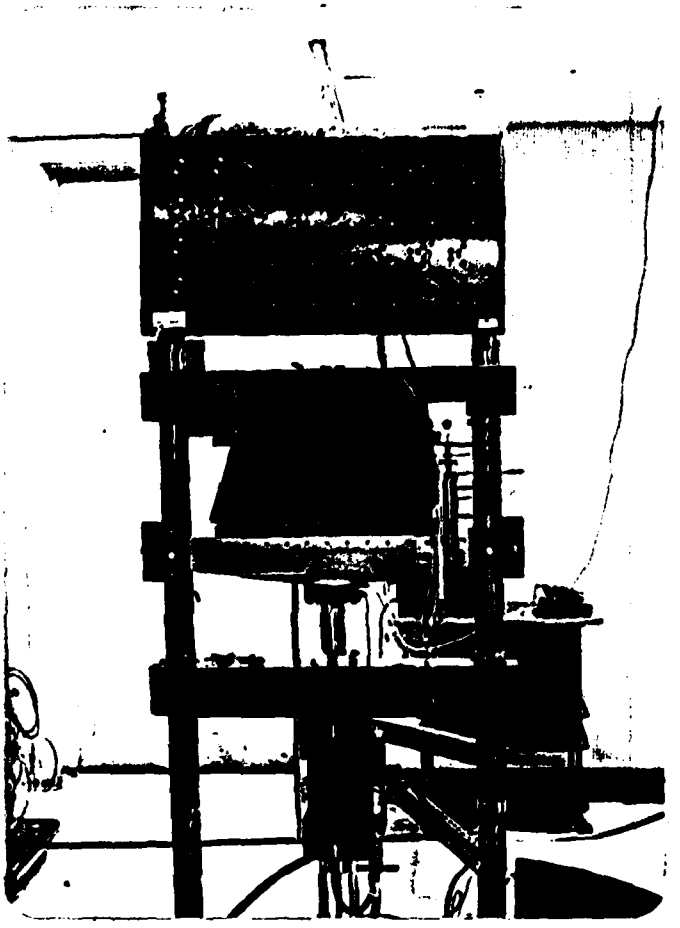

Figure 11 Complete Experimental Set-up

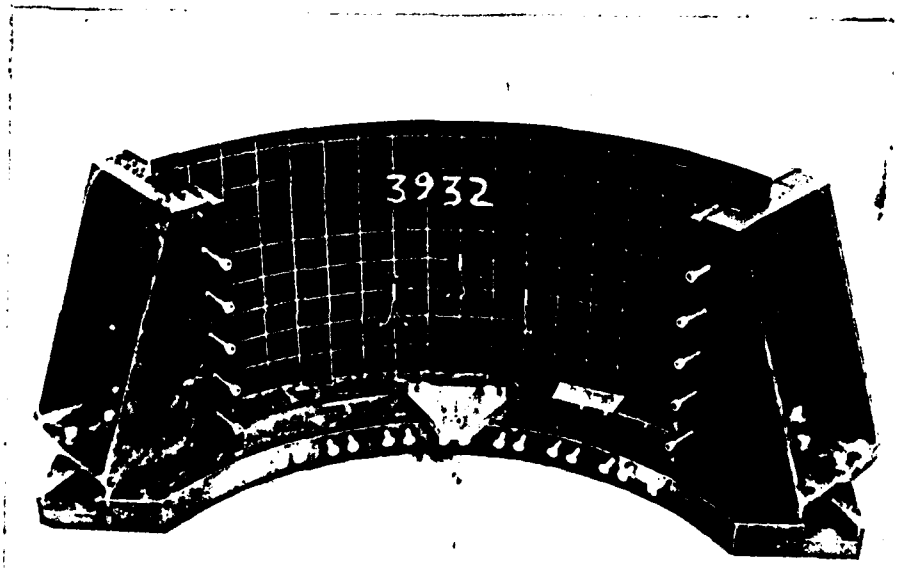

Figure 12 Panel Support Fixture with Panel Installed

One might observe the vertical LVDT (Linear Variable Differential Transducer) located on the right side of the set-up in Fig. 11, used to measure panel end-shortening. Furthermore, a matrix of LVDT's have been placed horizontally on the back of the panel as shown in Fig. 13, to measure radial displacements. Additionally, 6 axial strain gages (back-to-back in 3 locations) were attached to each of the 30 panels.

Included within the experimentation is:

1. determination of buckling load,
2. strain measurements on inner and outer faces of the panel at discretely located positions,
3. radial displacement measurements.

These three measurements were incorporated into three techniques for determining the buckling load

1. load vs end-shortening,
2. strain reversal,
3. Southwell Plot (see Appendix A).

Each set of measurements were carried out for all 30 panels. The data was stored in a CEL 86 Computer in a real time mode and printed out later. The data was also displayed on a computer terminal CRT so that the load and displacements could be viewed during the testing.

Test Procedure

Once the panel was installed, the instrumentation (LVDT's and

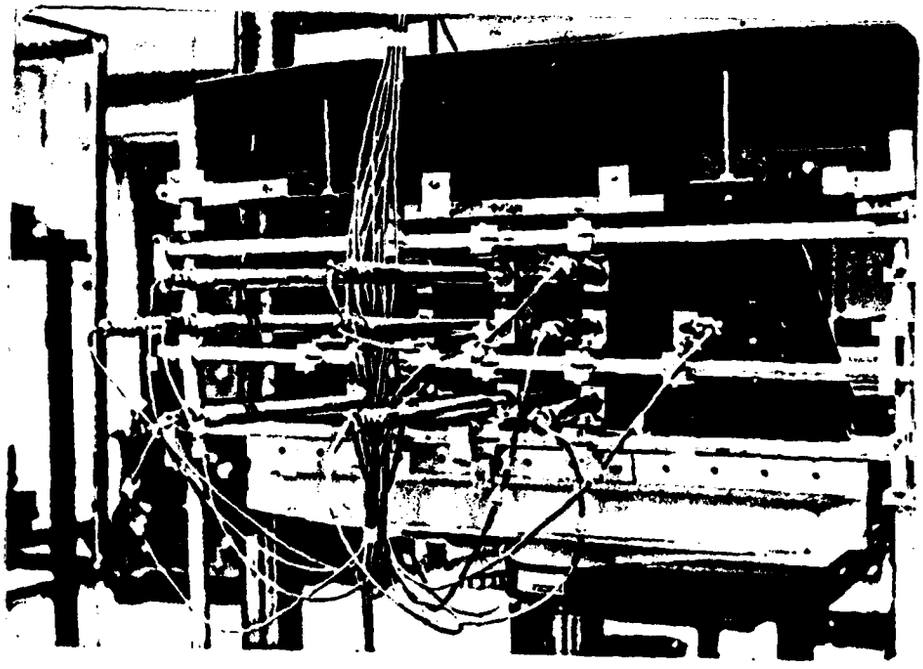

Figure 13 Horizontal LVDT's for Radial Displacement Measurements

strain gages) was zeroed out electronically and the test begun. The load was applied and the data was sampled two times per second for most of the panels. When the first major buckle occurred, the location was noted and the buckled pattern photographed. The loading was continued in order to get some portion of the postbuckling curve. When the top plate contacted the side supports, or when panel breakage made continued loading impractical, the load was removed.

V. RESULTS

Panel Identification

The panels used in this thesis are identified in the following manner:

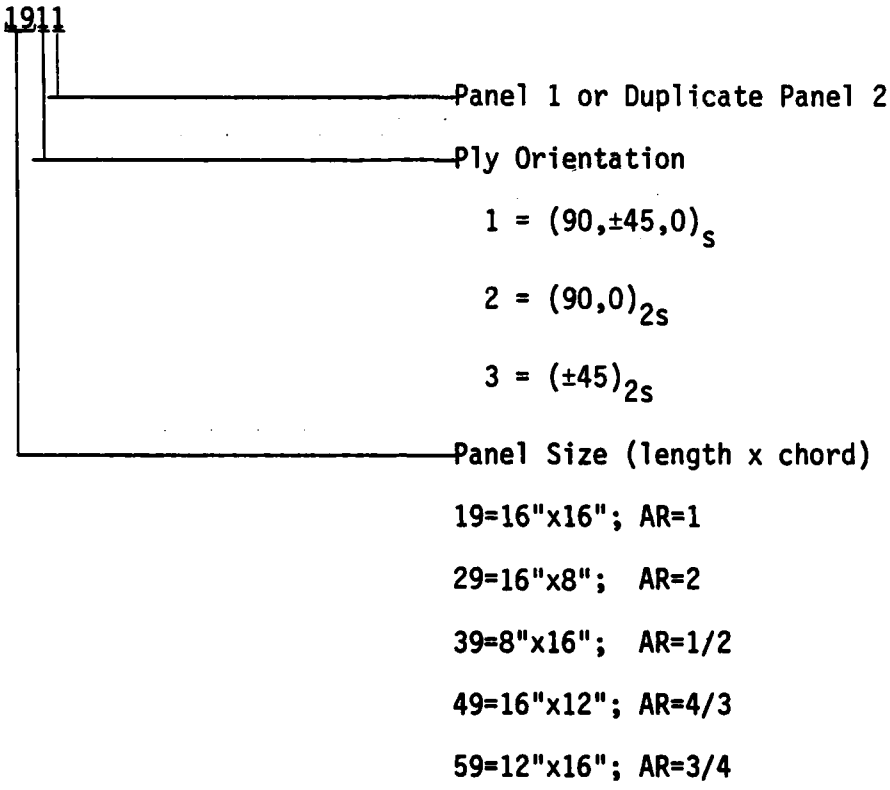

A three digit number is used when the average results of both duplicate panels are referenced. As an example, 392 means the average buckling load or end-shortening deflection of panels 3921 and 3922 are being referenced.

Experimental/Analytical Comparison

Table I shows the experimental and analytical results for all 30

panels tested. Table II is a summary of Table I, showing only the average knockdown factors associated with all three methods used to determine the buckling loads. The percent knockdown factor used in this thesis is defined as $(1 - \frac{\text{experimental buckling load}}{\text{analytical bifurcation load}}) \times 100$. The end-shortening technique (E-S), was the most reliable source of experimental data with knockdown factors ranging from 2.9% to 31.8%. The buckling load was determined to be that maximum load which caused the buckling configuration of the panel and a distinct drop-off in load on a plot of its load vs end-shortening curve. The load vs end-shortening curve for each panel is shown in Fig's. 14 to 27. From these curves it can be noticed that the panels do not have post-buckling strength, which was similarly reported by Becker [7]. Panel 1911 was not included in the analysis because panel breakage produced such scattered load vs end-shortening data that a linearization of the curve proved impractical. Panels 2921, 2922, 3922, and 5921 were not included in the calculation of E-S knockdown factors because their experimental buckling loads were higher than the analytical values. This was most likely due to panel cutting irregularities. These panels were cut a little wider than the rest of the panels producing a smaller clearance between the vertical edges of the panels and the back of the simple support device shown in Fig. 10. As the load was applied the panel's freedom of motion in the Y-direction was surpressed resulting in a stiffer panel. A new set of boundary conditions (with v=0) were programmed analytically. The re-

Panel ID	BUCKLING LOADS (LB) End-Shortening Method	Strain Reversal Method	Southwell Method	End Shortening (in)
1911	[1]	[1]	[1]	[1]
1912	5562.5	5592.1	5561.4	0.0606
1912	5288.5	4811.9	4182.1	0.0494
1922	5197.9	5112.0	[2]	0.0447
1931	4833.3	4838.9	[2]	0.0666
1932	5593.8	5587.5	[2]	0.0680
2911	2593.0	2570.0	1621.8	0.0601
2912	2764.0	2780.0	1945.8	0.0608
2921	2710.0[4]	2296.0	2569.3	0.0529
2922	2842.0[4]	[3]	2197.5	0.0517
2931	2610.0	2624.0	[2]	0.0749
2932	2670.0	2672.0	[2]	0.0770
3911	6305.6	6464.4	5996.7	0.0455
3912	6222.2	6183.9	5278.3	0.0525
3921	4559.5	4682.2	6491.4[4]	0.0449
3922	6066.7[4]	6000.0[4]	5815.0[4]	0.0450
3931	5978.3	5972.2	5735.5	0.0546
3932	4684.8	4766.7	[2]	0.0467
4911	3480.0	3287.0	3165.8	0.0623
4912	3844.4	3053.3	3333.8	0.0639
4921	3540.0	3548.0	3095.8	0.0476
4922	3825.6	[3]	[4]4161.39	0.0566
4931	4310.0	4311.1	[2]	0.0779
4932	4250.0	4250.0	[2]	0.0767
5911	5153.9	5154.0	6804.5	0.0427
5912	6435.0	6460.0	7468.6	0.0568
5921	5733.3[4]	[5]	4304.8	0.0402
5922	4375.0	4402.8	[2]	0.0321
5931	5384.6	5380.0	[2]	0.0633
5932	5076.9	5076.9	[2]	0.0553

Table I. Panel Experimental Buckling Loads

Table I Key

1. Panel Breakage Procluded Meaningful Data
2. Linear Relationship of Ld vs Circumferential Displ.
3. Unreducable Data
4. Buckling Load Higher Than Analytical Bifurcation Load
5. Strain Gages Not Placed Back-to-Back

Aspect Ratio	Panels	Analytical Bifurcation Load (lb)	End-Shortening Method Buckling Load (lb)	Knockdown[1] Factor (%)	Southwell[2] Knockdown Factor (%)	Strain Reversal[3] Knockdown Factor (%)
16 x 16	191	7462.9	5562.5[4]	25.5	25.5	25.1
1	192	5398.1	5243.2	2.9	22.5[7]	8.1
	193	6195.1	5213.6	15.8	[8]	15.9
16 x 8	291	3512.3	2678.5	23.7	49.2	23.8
2	292	2510.7	2776.0[5]	[5]	12.5[9]	8.6[10]
	273	3018.0	2640.0	12.5	[8]	12.3
8 x 16	391	7641.5	6263.9	18.0	26.2	17.2
$\frac{1}{2}$	392	5634.0	4559.5[6]	19.1	[8]	16.9[6]
	393	6537.0	5331.6	18.4	12.3[11]	17.9
16 x 12	491	5372.3	3662.2	31.8	39.5	41.0
$\frac{4}{3}$	492	4115.5	3682.8	10.5	24.8[12]	13.8[13]
	493	4510.9	4280.0	5.1	[8]	5.1
12 x 16	591	7506.4	5794.5	22.8	4.9	22.6
$\frac{3}{4}$	592	5478.6	4375.0[16]	20.1	21.4[14]	19.6[15]
	593	6289.5	5230.8	16.8	[8]	19.9

Table II. Average Knockdown Factors

Table II Key

1. $1 - \frac{\text{End-Shortening Buckling Load}}{\text{Analytical Bifurcation Load}}$
2. $1 - \frac{\text{Southwell Buckling Load}}{\text{Analytical Bifurcation Load}}$
3. $1 - \frac{\text{Strain Reversal Buckling Load}}{\text{Analytical Bifurcation Load}}$
4. Panel 1911 not included due to breakage
5. Both 2921 and 2922 had higher experimental buckling loads than analytical
6. 3922 not included; higher than analytical load
7. 1922 not included; linear data
8. Linear data for both panels
9. 2921 not included; higher than analytical load
10. 2922 not included; unreducable data
11. 3932 not included; linear data
12. 4922 not included; Southwell load higher than analytical
13. 4922 not included; unreducable data
14. 5922 not included; linear data
15. 5921 not included; strain gages not placed back-to-back
16. 5921 not included; higher than analytical load

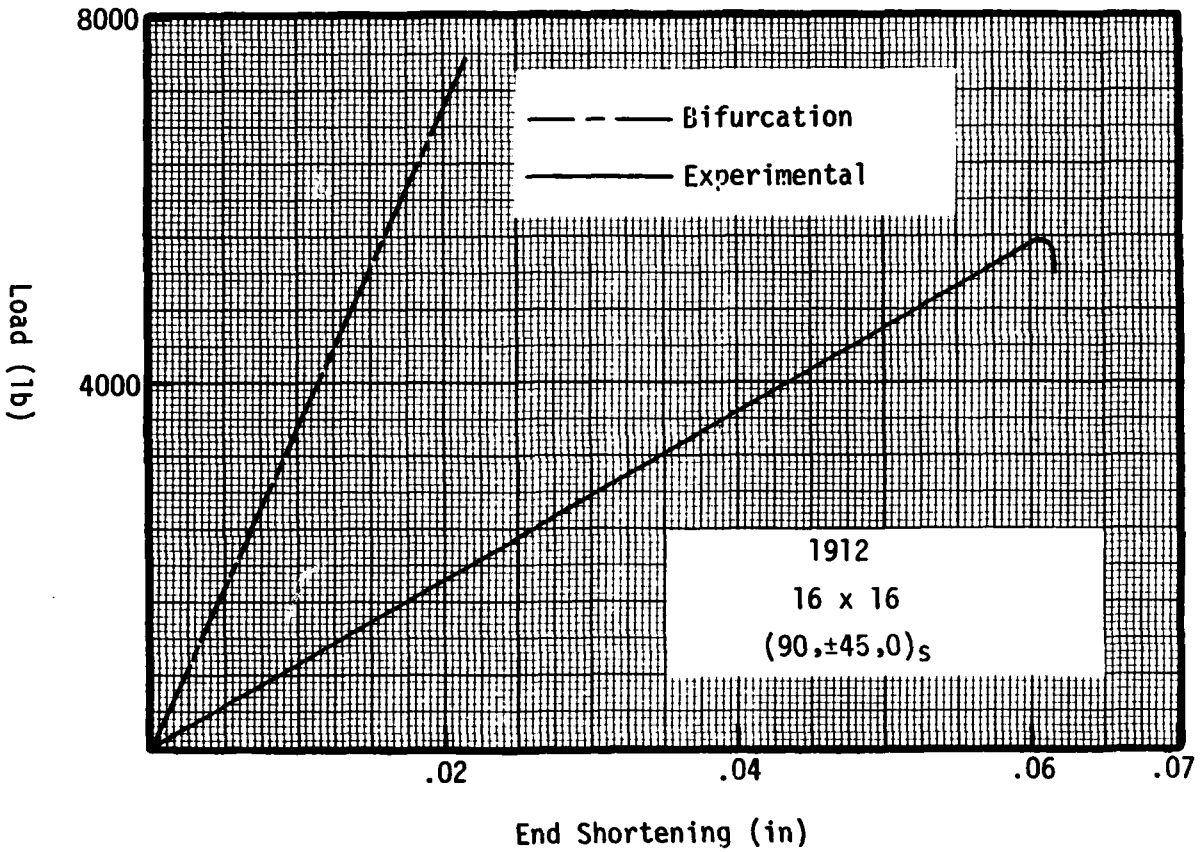

Figure 14 Analytical and Experimental Results for 1912 Panel

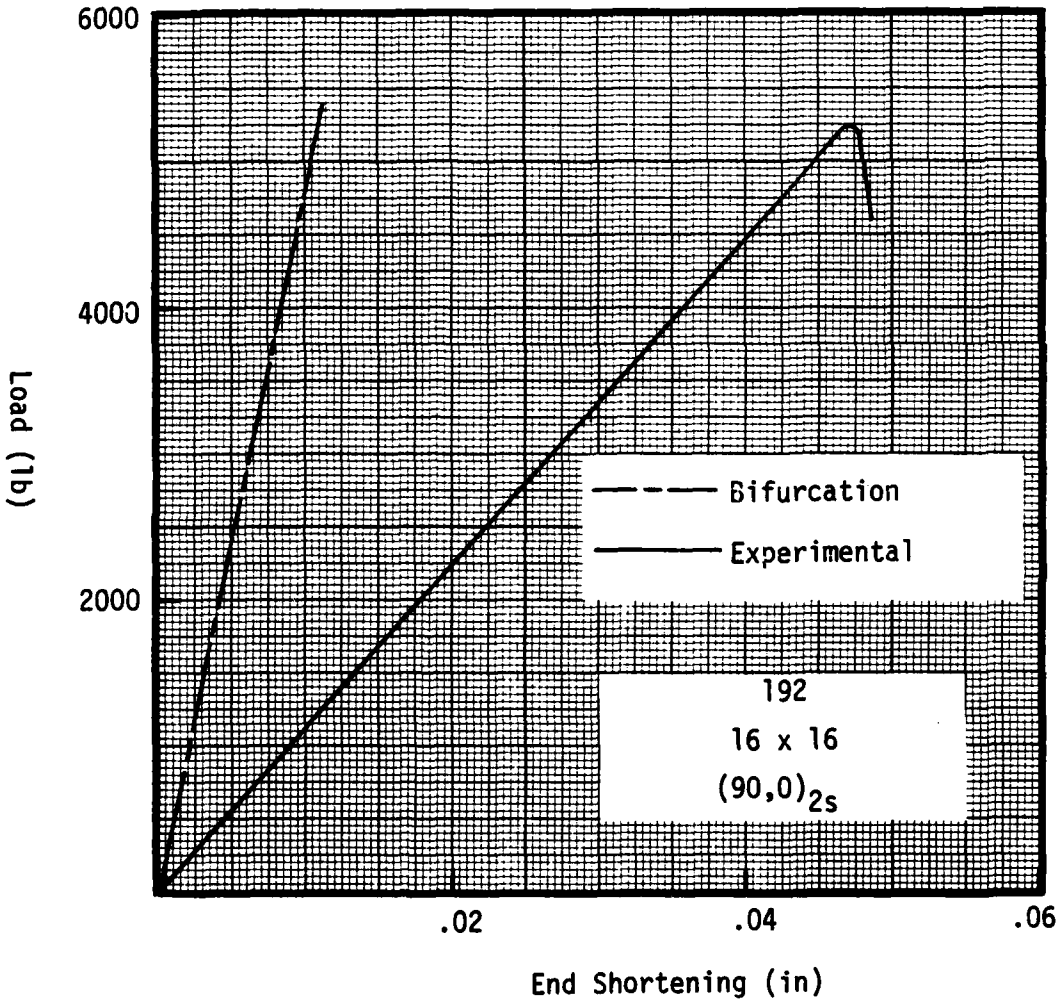

Figure 15 Analytical and Experimental Results for 192 Panel

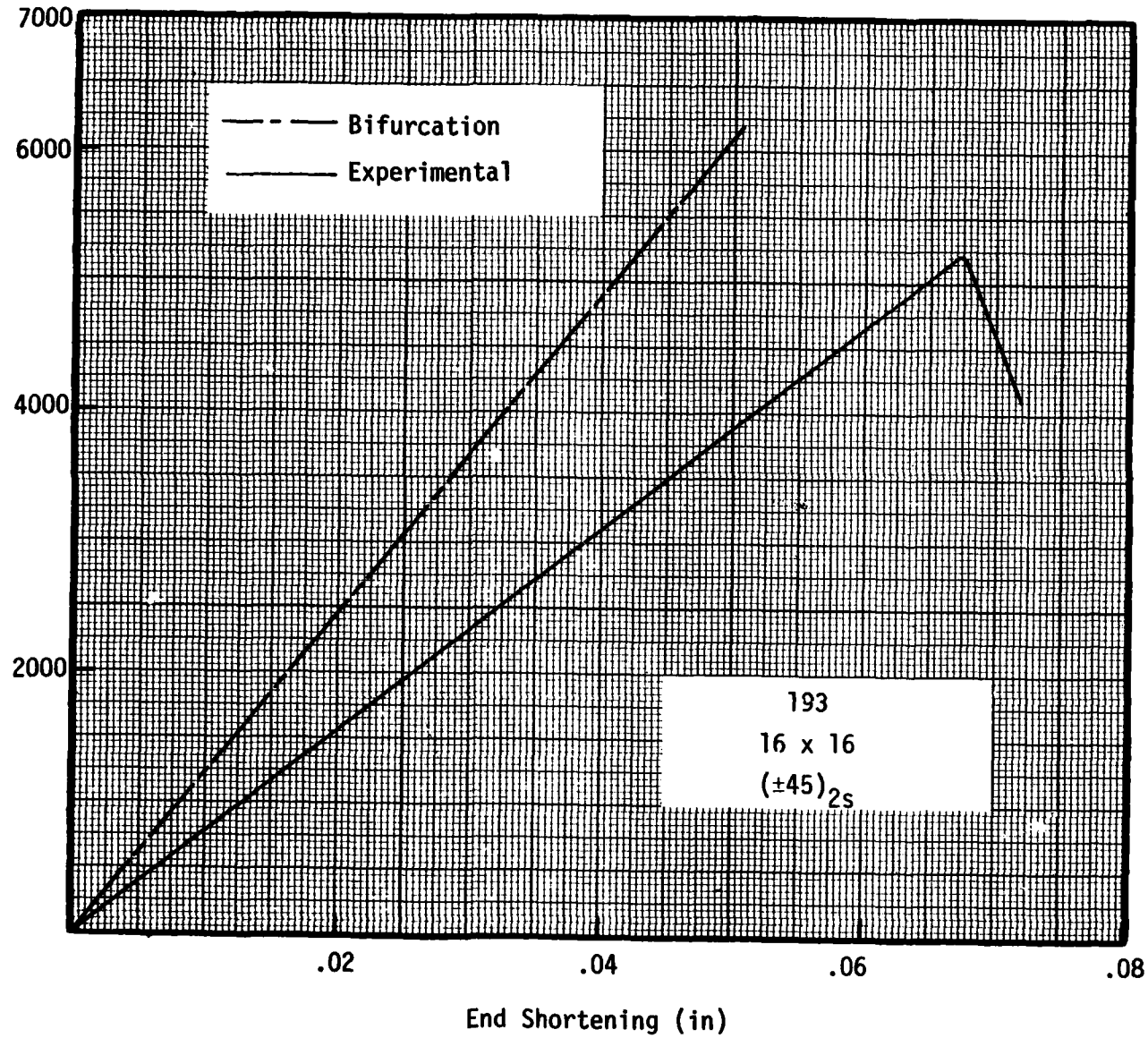

Figure 16 Analytical and Experimental Results for 193 Panel

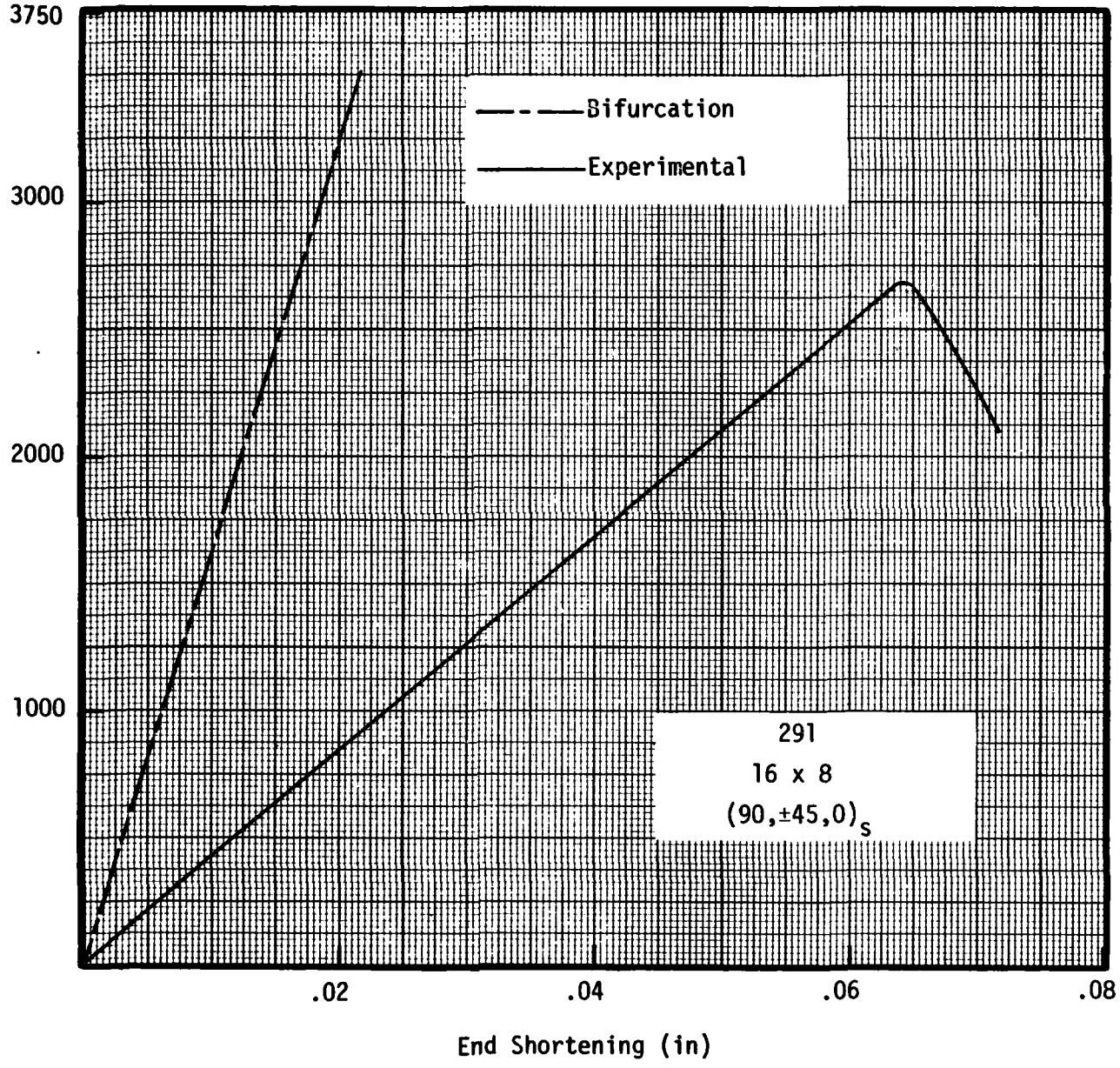

Figure 17 Analytical and Experimental Results for 291 Panel

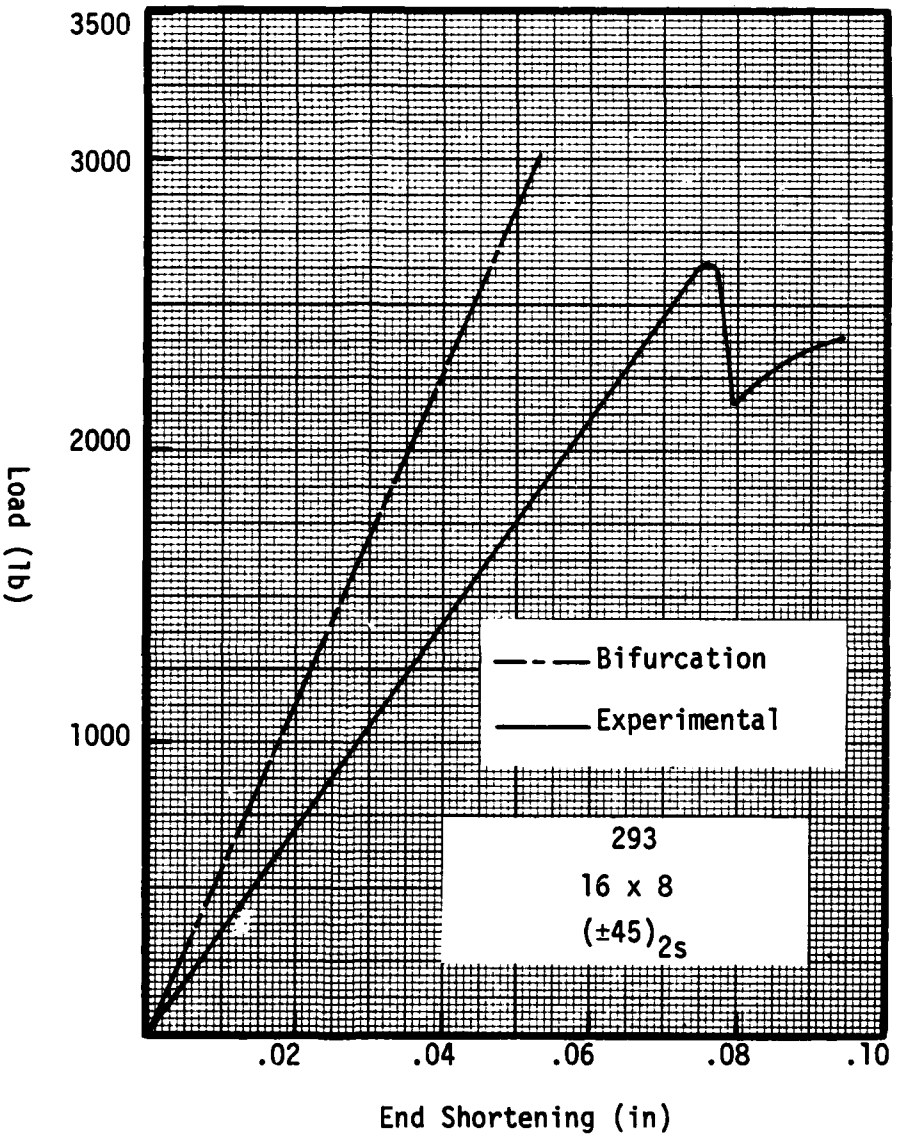

Figure 18 Analytical and Experimental Results for 293 Panel

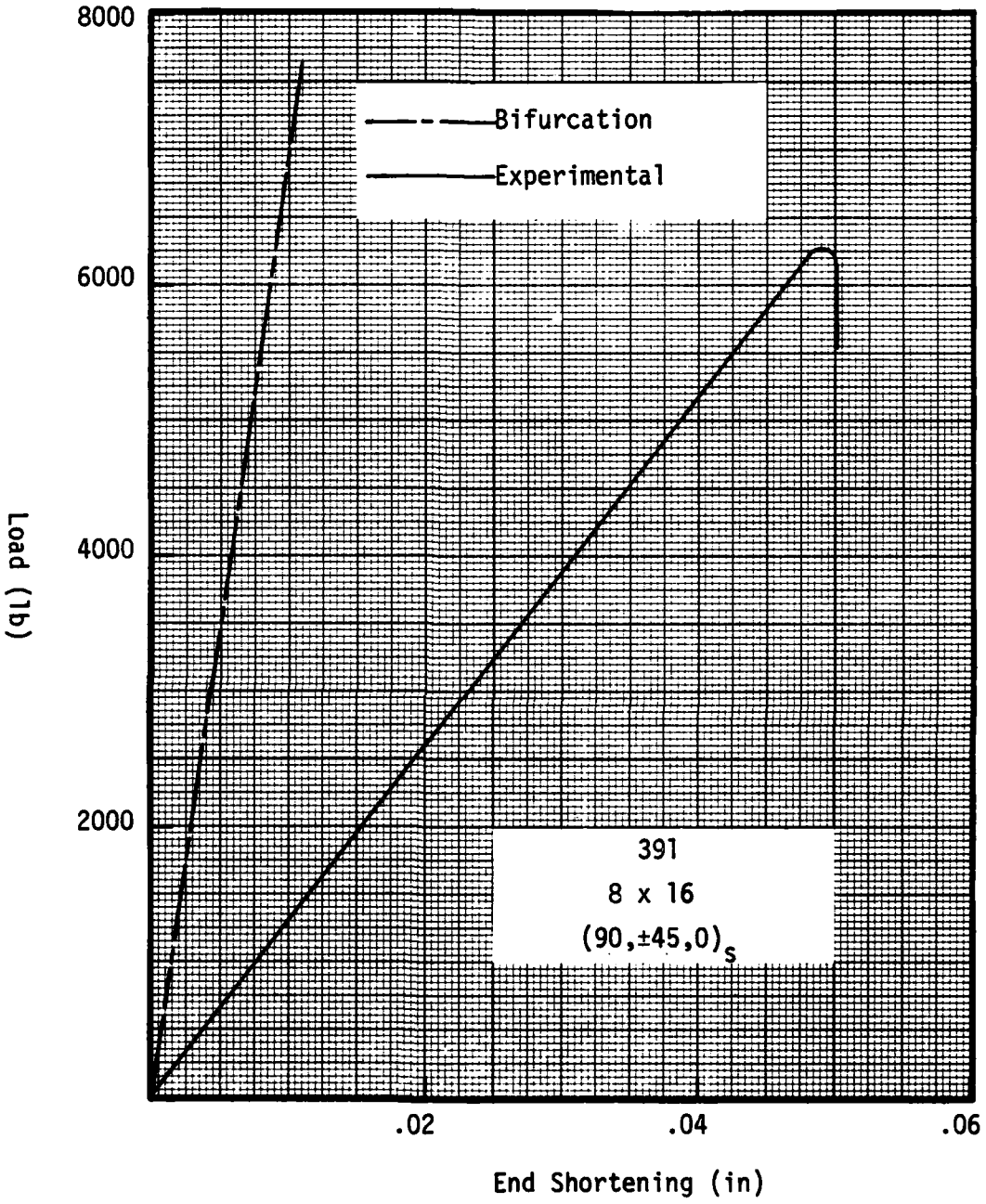

Figure 19 Analytical and Experimental Results for 391 Panel

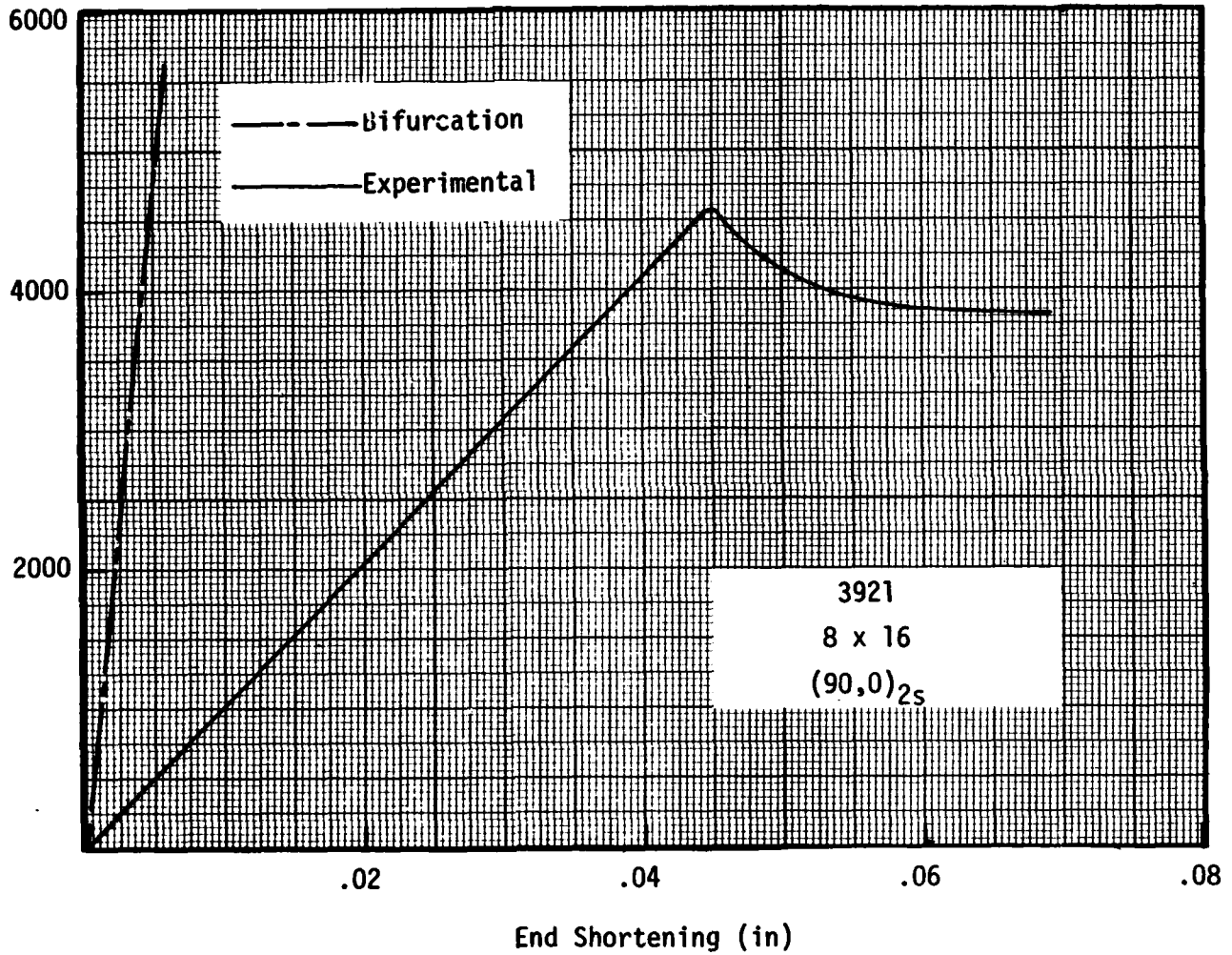

Figure 20 Analytical and Experimental Results for 3921 Panel

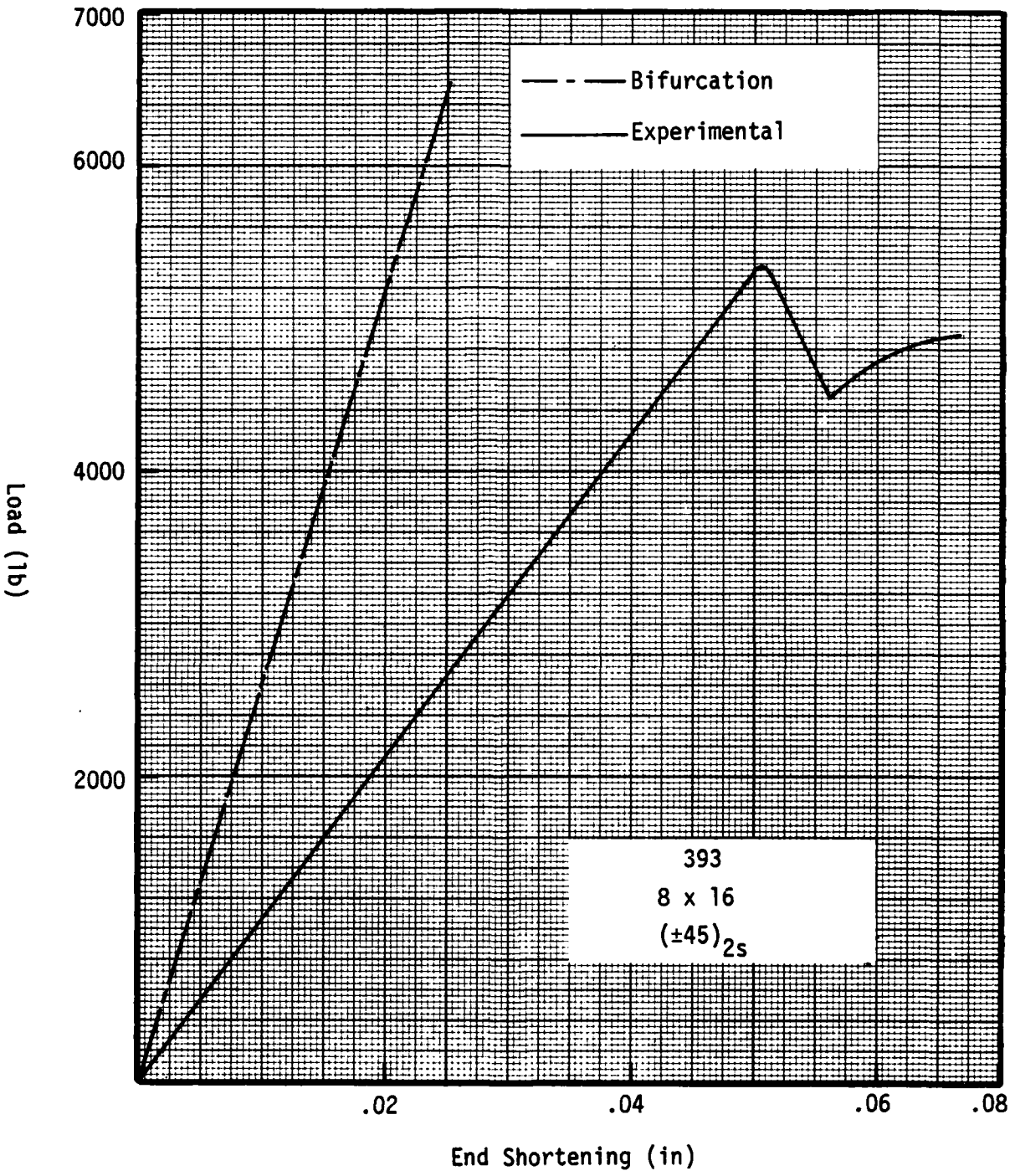

Figure 21 Analytical and Experimental Results for 393 Panel

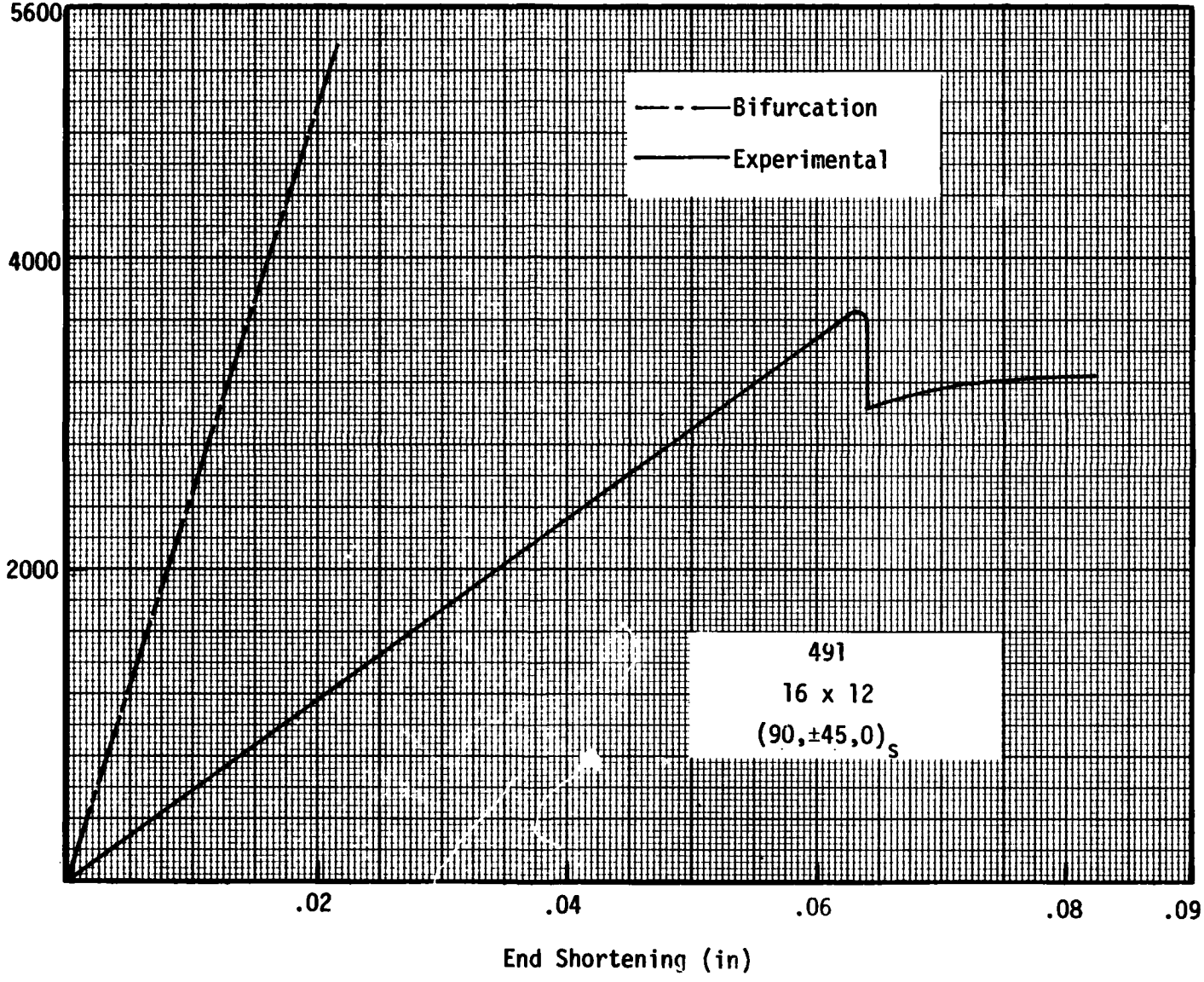

Figure 22 Analytical and Experimental Results for 491 Panel

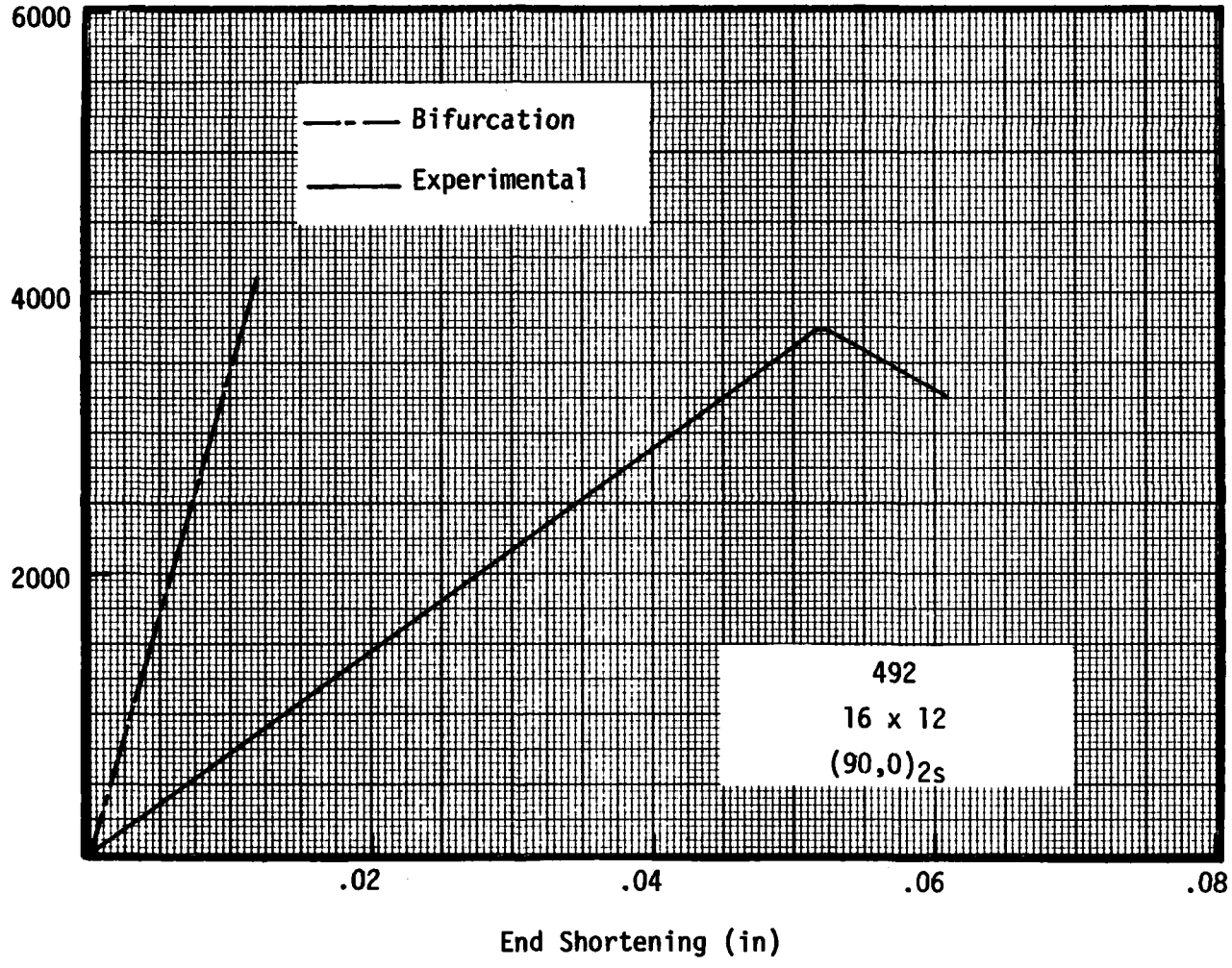

Figure 23 Analytical and Experimental Results for 492 Panel

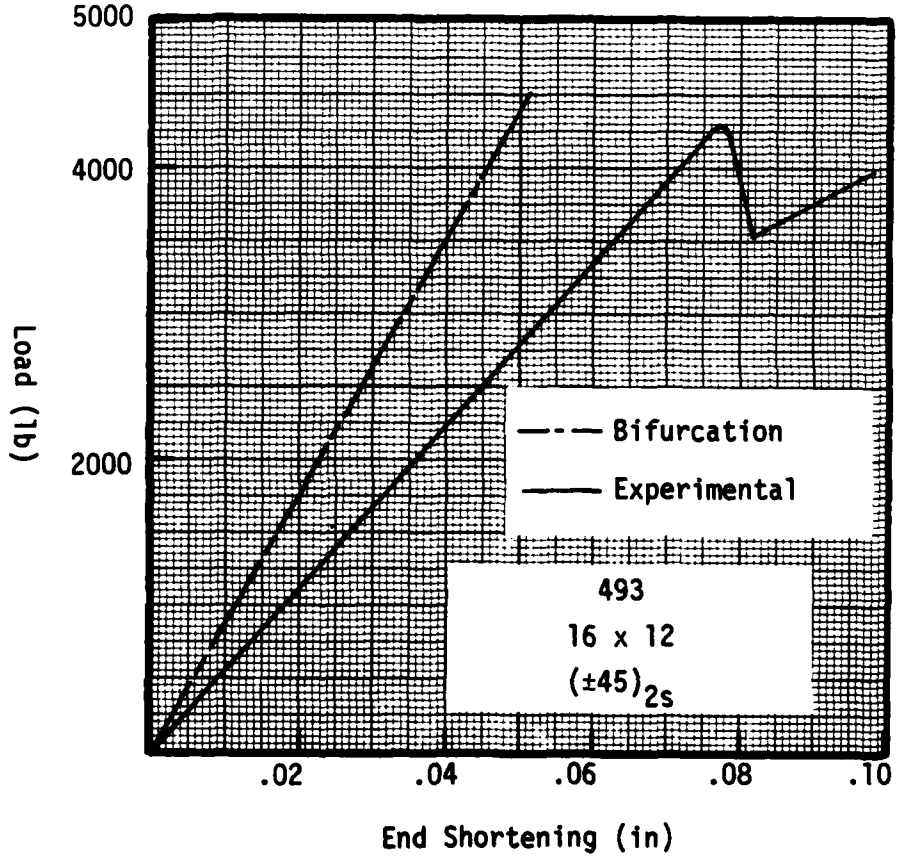

Figure 24 Analytical and Experimental Results for 493 Panel

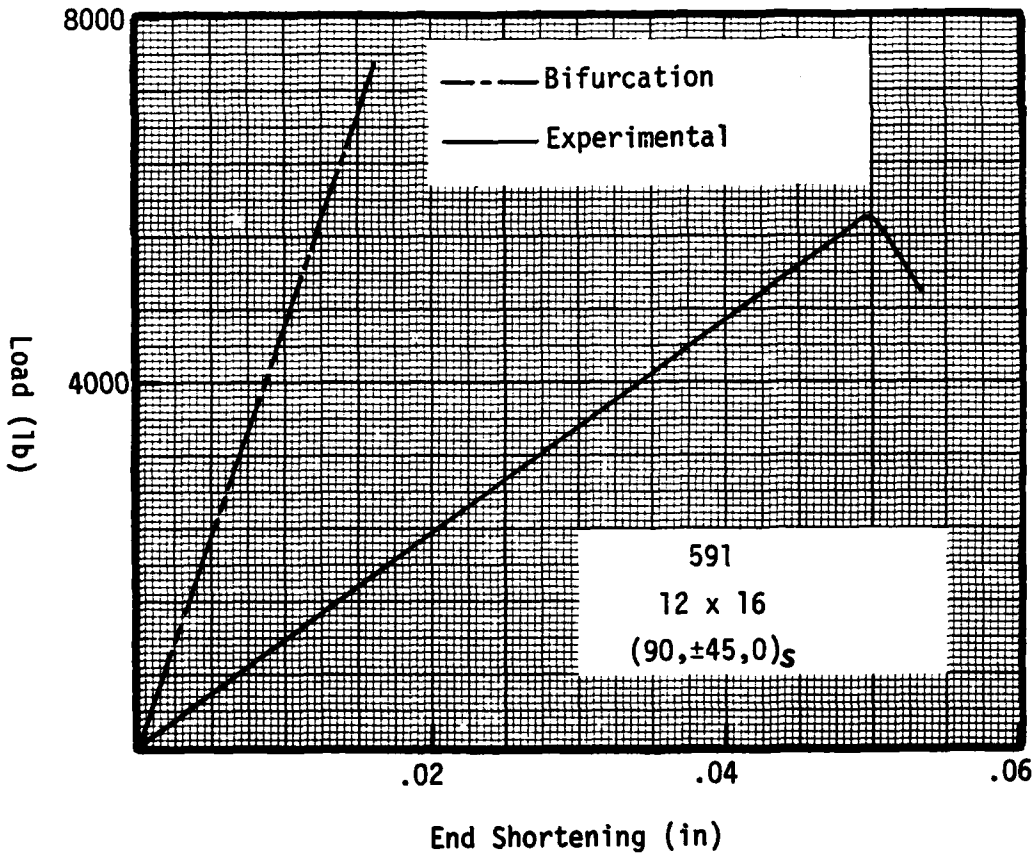

Figure 25 Analytical and Experimental Results for 591 Panel

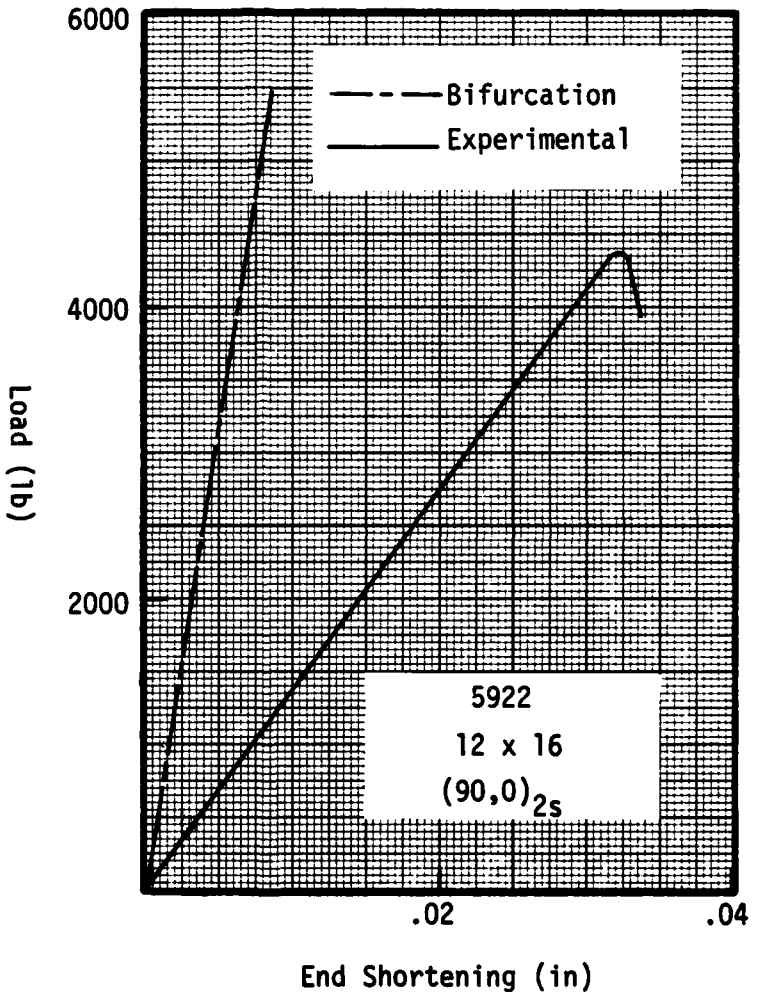

Figure 26 Analytical and Experimental Results for 5922 Panel

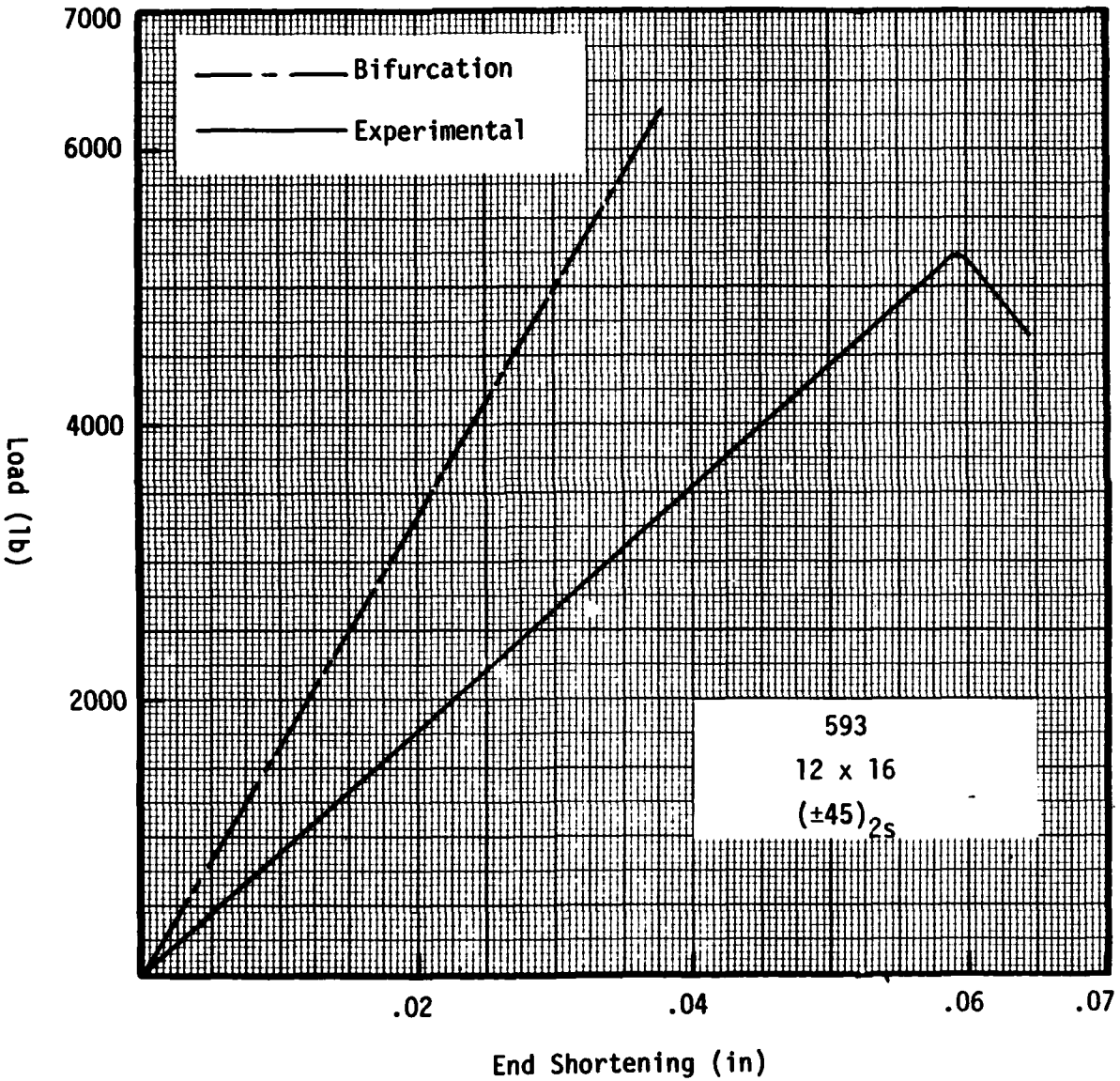

Figure 27 Analytical and Experimental Results for 593 Panel

sulting analytical bifurcation loads were, in fact, higher than the experimental buckling loads. This indicates that the actual experimental boundary conditions for these four panels did not correspond to the desired simple support conditions. The knockdown factors associated with the new boundary conditions (v=0) were 11% and 13.7% for the 292 and 5921 panels, respectively.

The strain reversal technique (S-R) provided a good check of the E-S method, with knockdown factors ranging from 5.1% to 41%. However, S-R was particularly susceptible to computer channel "noise" which on occasion produced unreducable data. Figure 28 shows a diagram of the strain reversal process. As the load is increased, the back-to-back strain gages register essentially the same increase in strain values. When buckling occurs, the strains of the respective gages increase dramatically in both tension and compression. The idealization of Fig. 28 is obtained experimentally only if the strain gages are located at a buckle. This implies that a prior knowledge of the buckling pattern is necessary. The strain gage placement for all 30 panels was based upon a symmetrical pattern about the panel's center as was indicated by STAGSC-1. As will be explained later, the actual pattern did not have this symmetry which meant that in most cases, the strain gages were not located at a buckle. However, good results were still obtained even though the plots of strain vs. load were not as well defined as in Fig. 28.

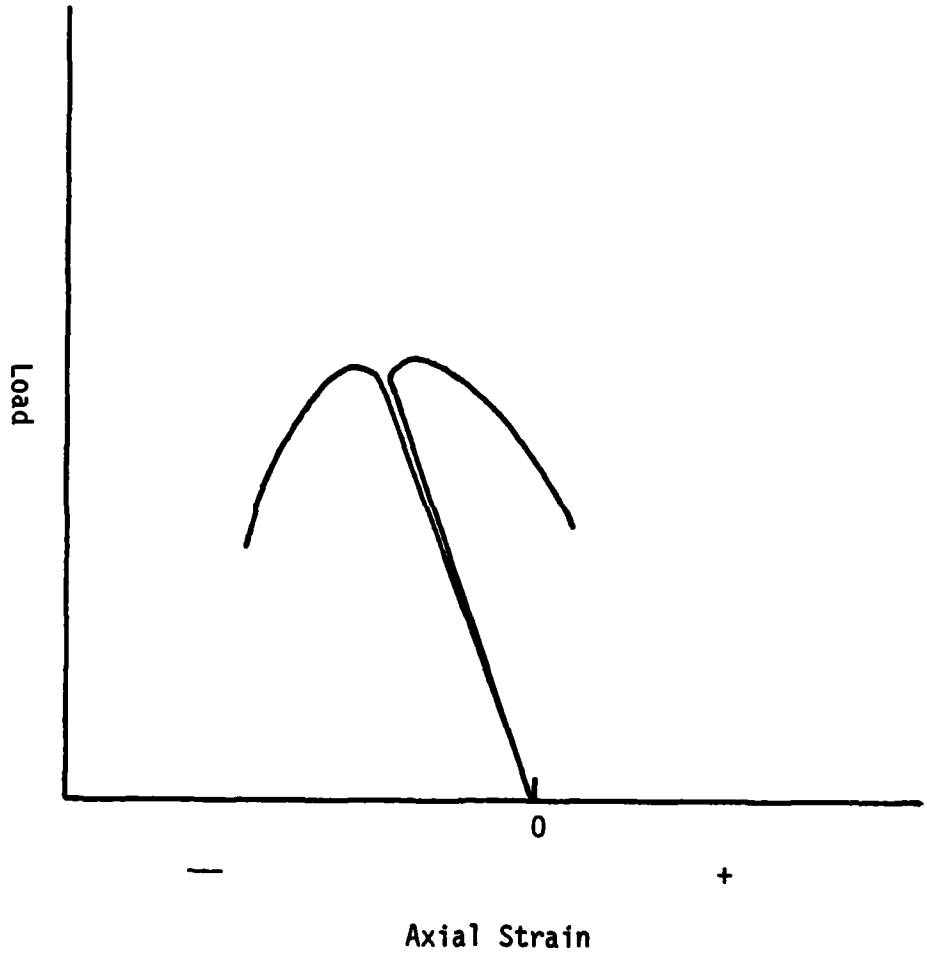

Figure 28 Strain Reversal Process

The least reliable method of determining the buckling load was the Southwell method. The Southwell method (see Appendix A for a fundamental discussion) required that the horizontal LVDT's be placed in very close proximity to the largest buckle. Since a matrix made up of nine and at times twelve LVDT's was used, this requirement was usually met. On a number of panels (see Table I) this method gave obviously erroneous results. This was due to a linear relationship of applied load to radial displacement. Only with those data plots that exhibit a nonlinear curve could a reasonable buckling load be obtained. The linearity may be explained by the combination of panel imperfections and panel support system eccentricities which serve to strengthen the panel. This prevented the relatively larger displacements at high load levels.

In order to measure radial eccentricities, a crude measuring device was made which was used in conjunction with a set of dial vernier calipers, see Fig. 29. The device was used to determine panel "out-of-roundness" brought about by less than perfect simple support installation. Radial measurements were taken at discrete locations on 11 panels. It was found that the final buckled configuration of these panels generally correspond to the pattern of their respective prebuckled radial eccentricities.

Buckling Pattern

It was found that the installation sequence of a panel into the test

Figure 29 Panel Measuring Device

set-up was crucial to the formation of its buckling pattern. Fig's. 30 to 41 show the buckling pattern progression of various panels as compared to the pattern generated by STAGSC-1. Notice that the experimental pattern did not exhibit the symmetry that theory would suggest. In fact, when the vertical supports were positioned as in Fig. 12 with the panel protruding ¼ of an inch at the top of the supports, none of the panels showed any buckling in their lower half. This is probably due to the panel's inherent flexibility in the upper half brought about by the unsupported ¼ inch space on each side. The result is an uneven stress distribution from the flexible upper half to the stiffer bottom half, thus preventing buckling at the bottom. The top picture in Fig's. 31, 35, 36, 38, and 40 shows the initial, small buckle which formed at the upper right portion of most of the panels tested. This buckle manifested itself as only a 1 to 2 percent drop-off in load, or a kink in the load vs end-shortening data. As the load was increased, the buckle progressed from right to left until a very audible and visual snap occurred signifying panel collapse and a distinct drop-off in load. The resulting buckling pattern was generally observed to contain three half-sine waves in the circumferential direction for the 16 and 12 inch chord length panels and one half-sine wave for the 8 inch chord panels. This is compared to the analytical patterns (Fig's. 32, 34, 37, 39, and 41) which, depending upon aspect ratio and ply orientation, contain 3 to 6 half-sine waves in the circumferential direction and 4 to 12 half-sine waves in the vertical direction. The formation of the initial

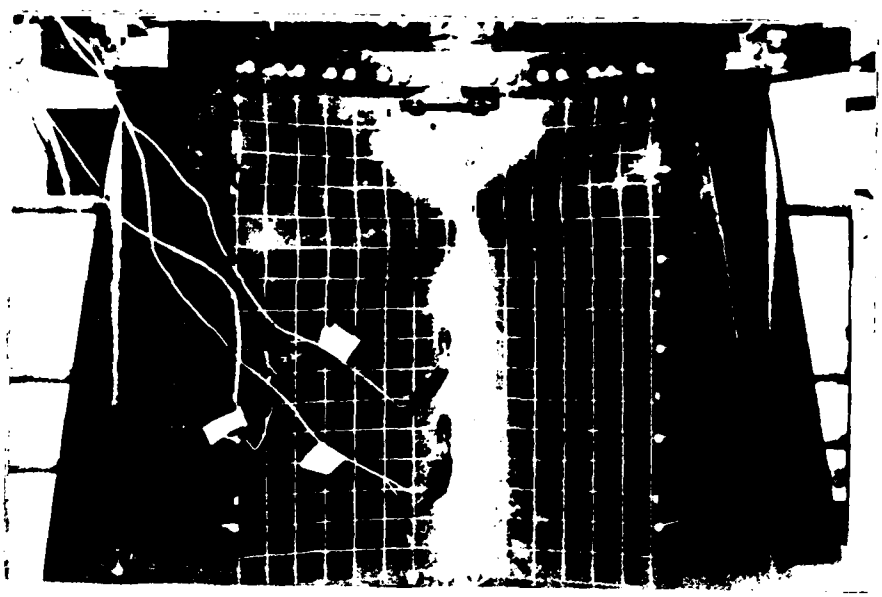

Figure 30 Buckling Pattern for 1911 Panel

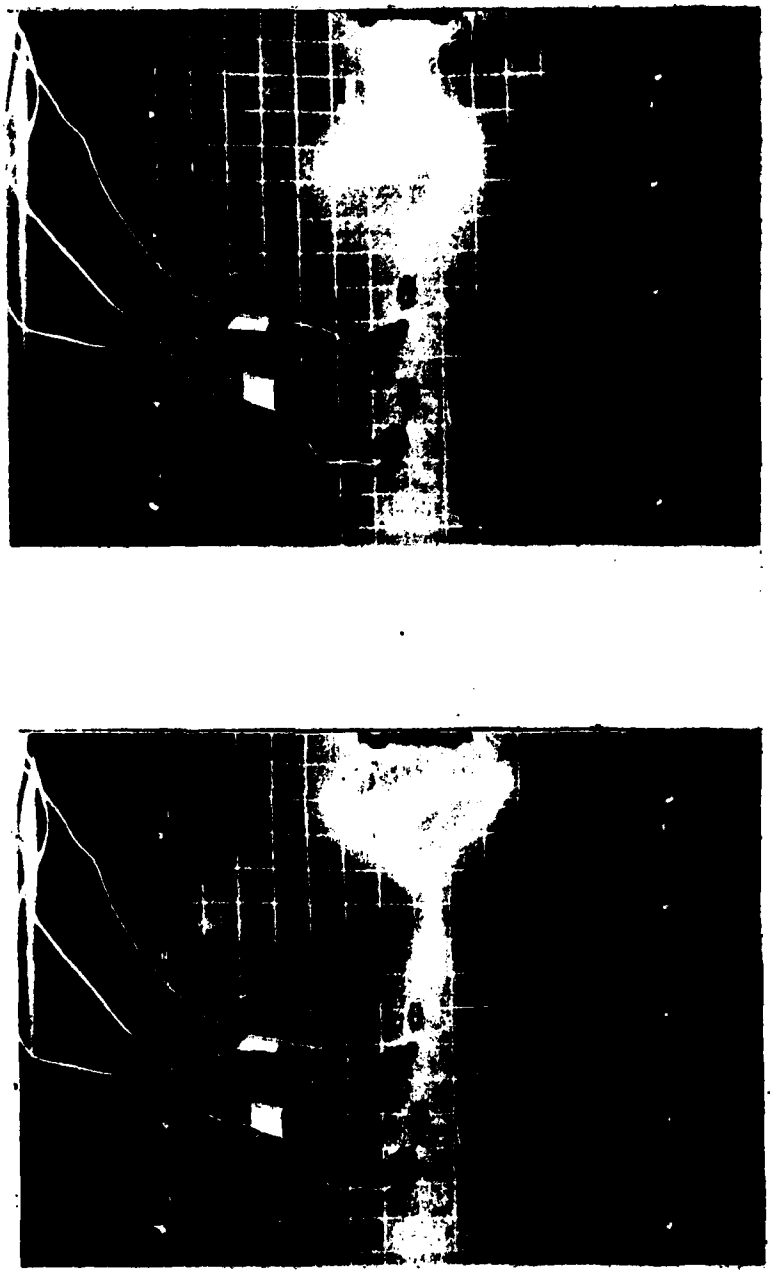

Figure 31 Buckling Progression for 1912 Panel

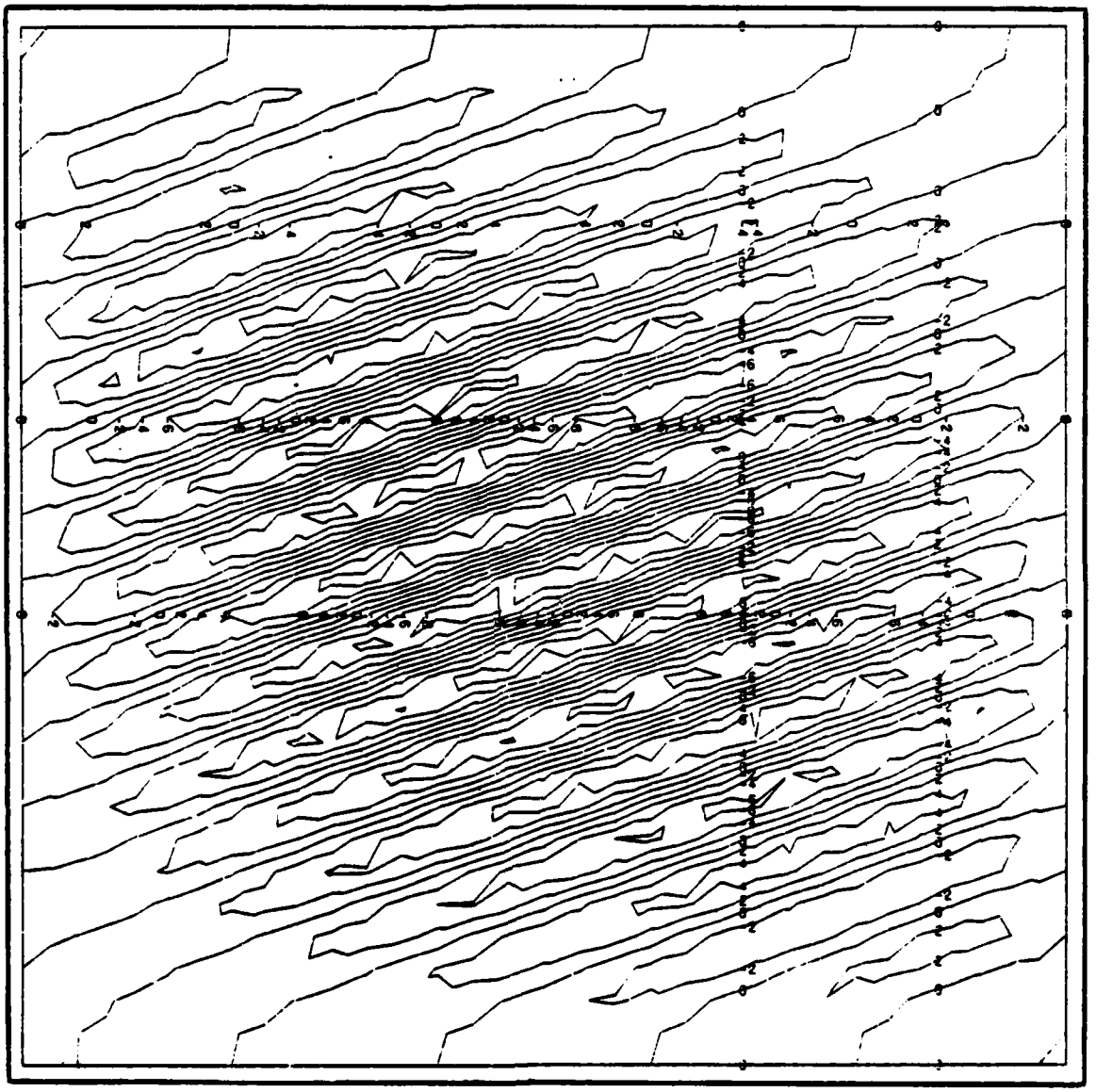

Figure 32 Analytical Buckling Pattern for 191 Panels

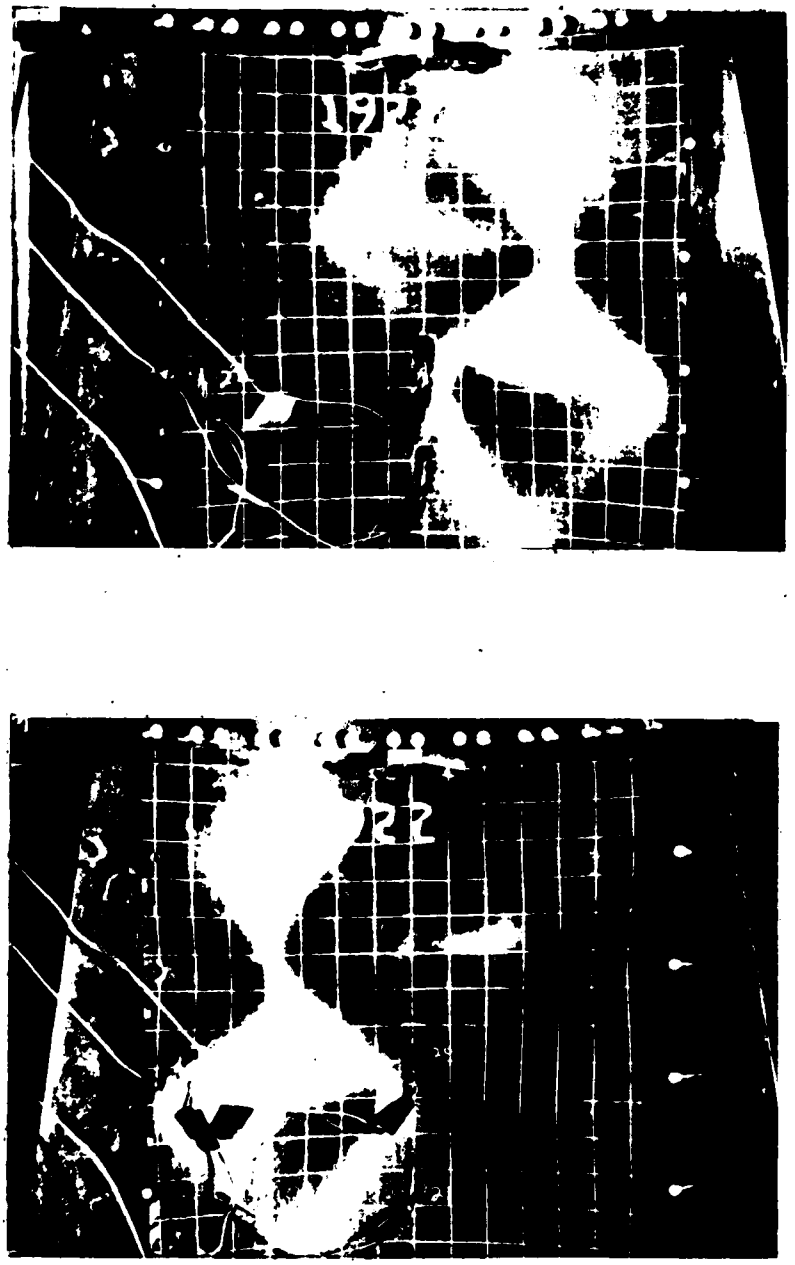

Figure 33 Buckling Progression for 1922 Panel

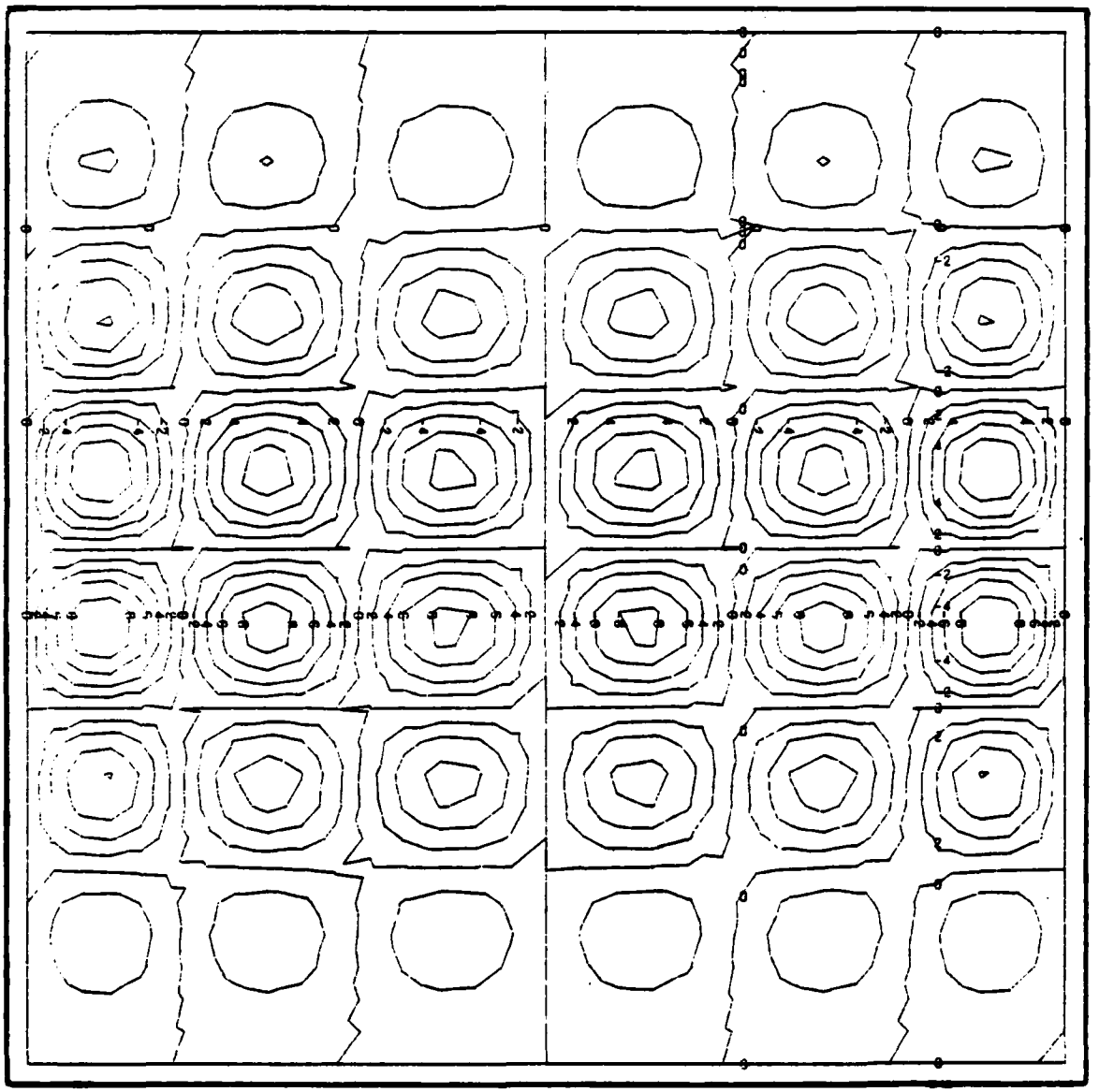

Figure 34 Analytical Buckling Pattern for 192 Panels

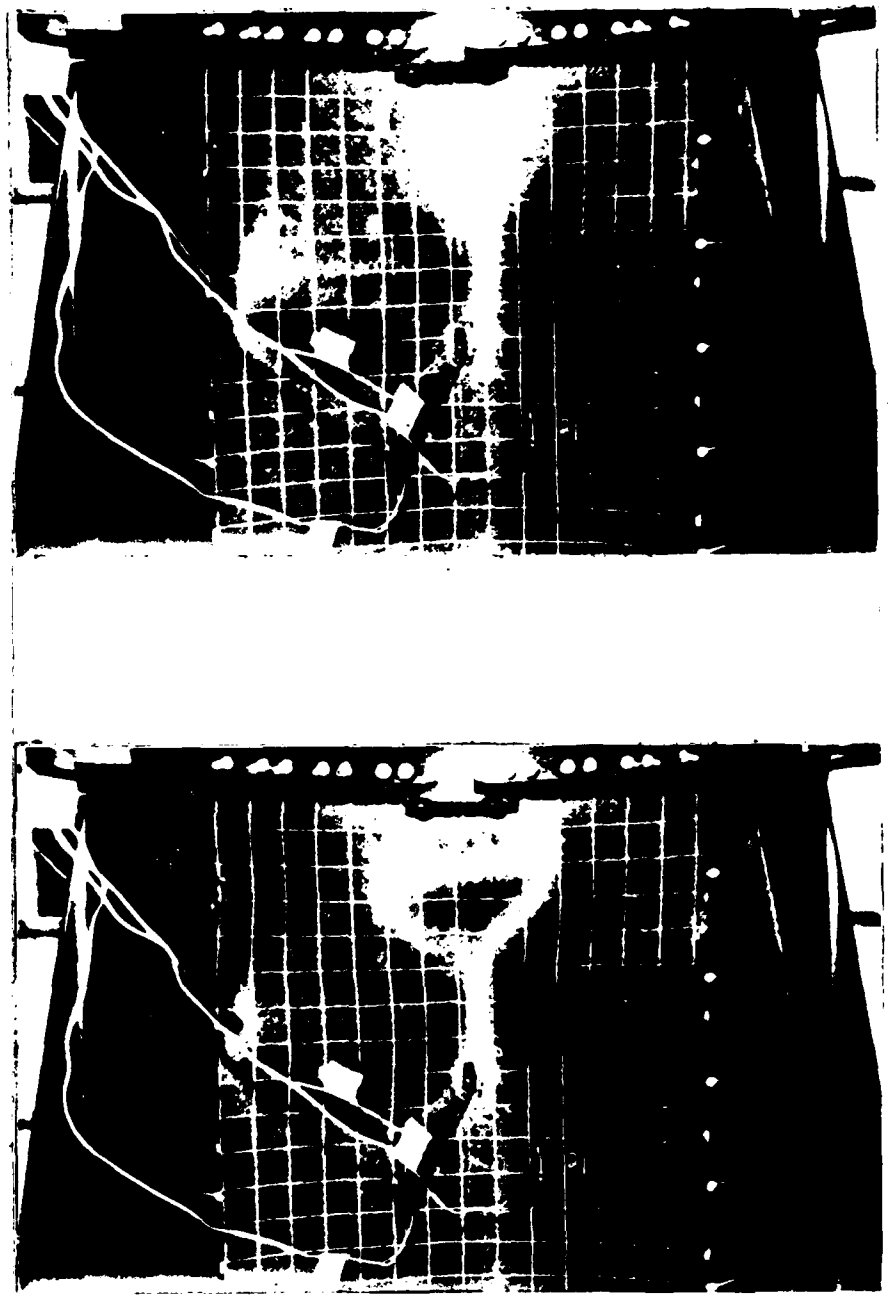

Figure 35 Buckling Progression for 1932 Panel

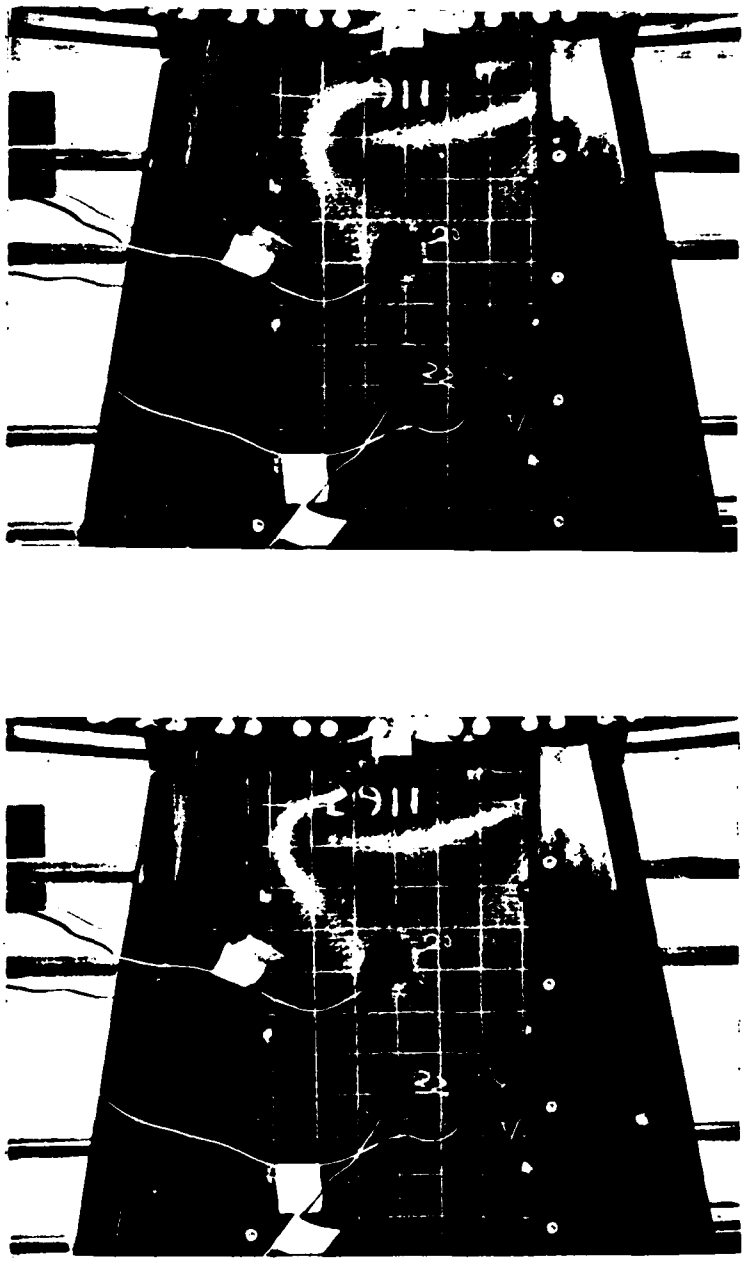

Figure 36 Buckling Progression for 2911 Panel

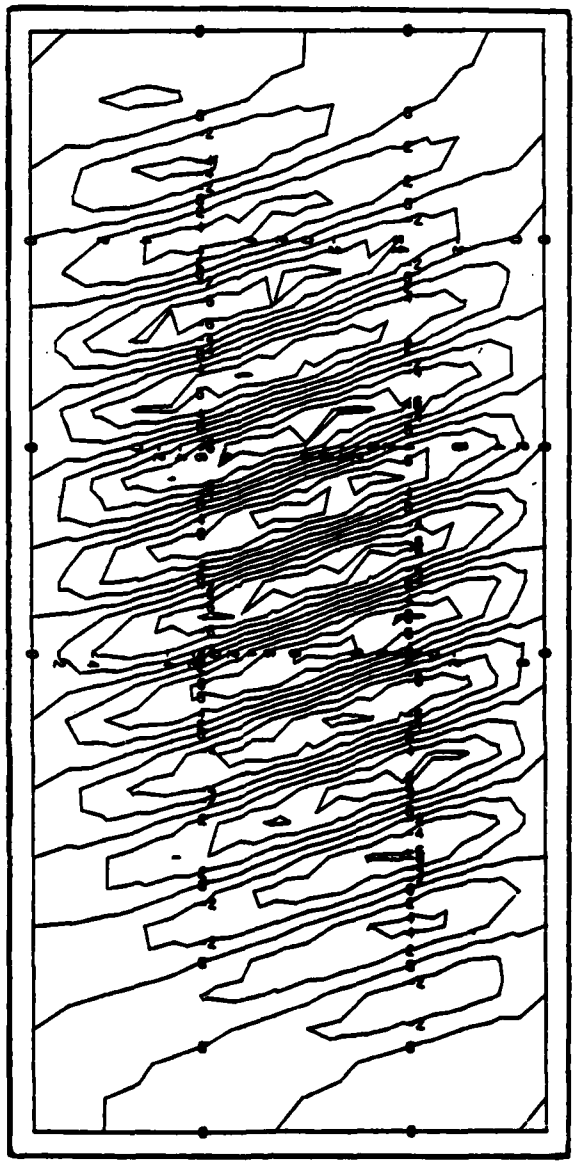

Figure 37 Analytical Buckling Pattern for 291 Panels

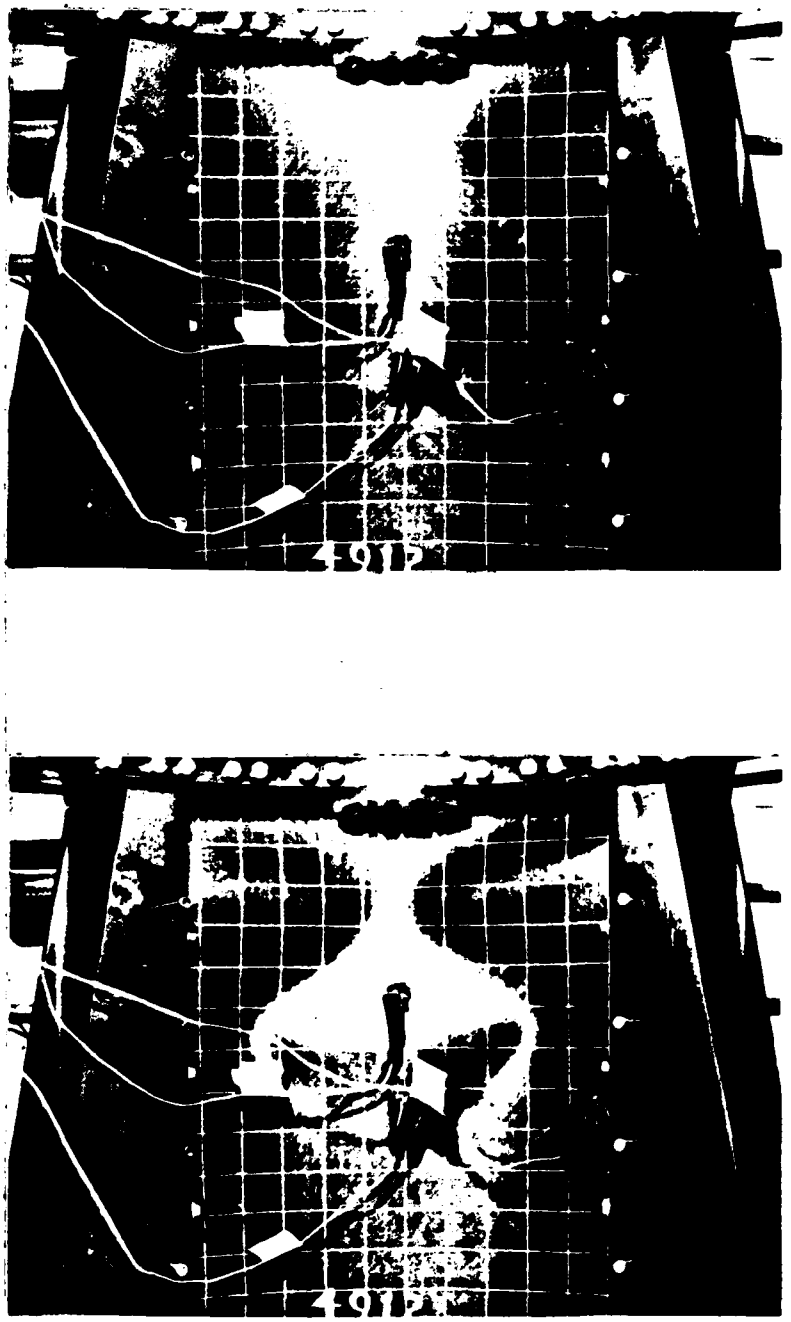

Figure 38 Buckling Progression for 4912 Panel

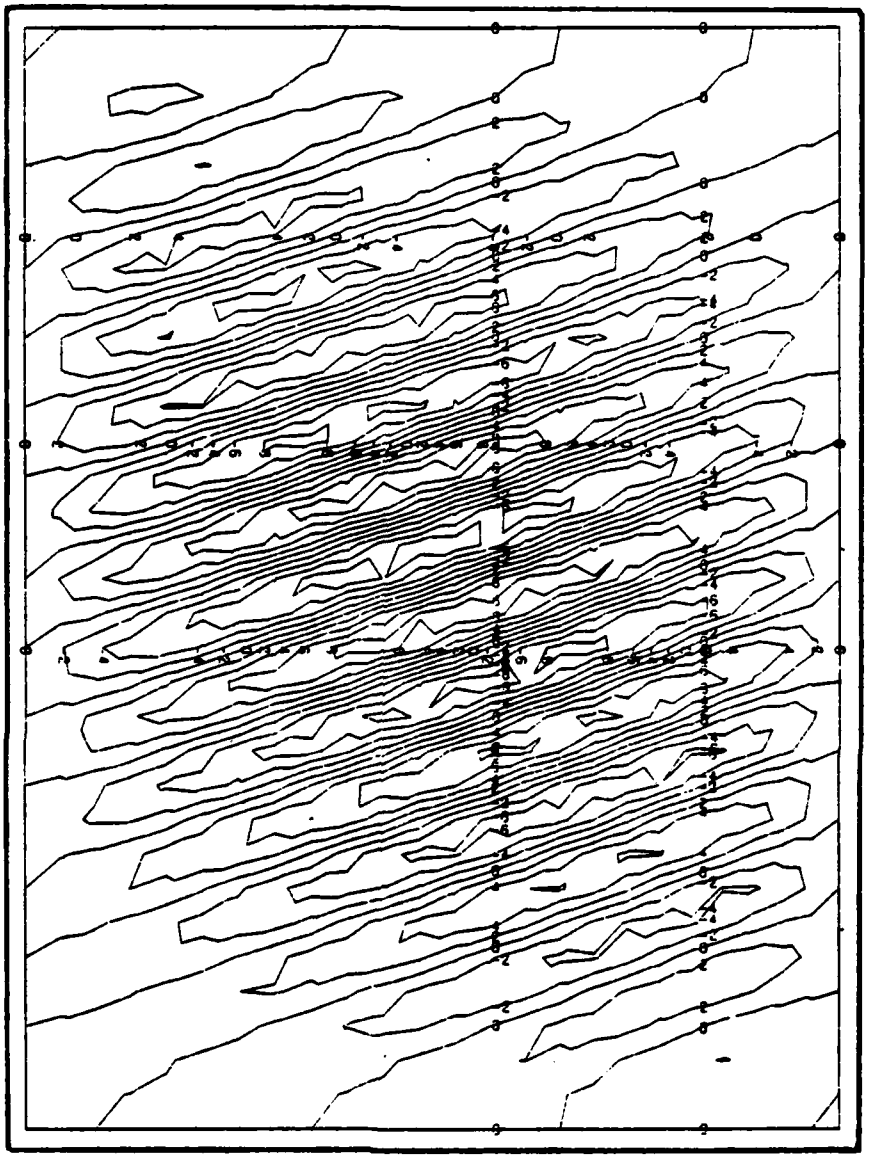

Figure 39 Analytical Buckling Pattern for 491 Panels

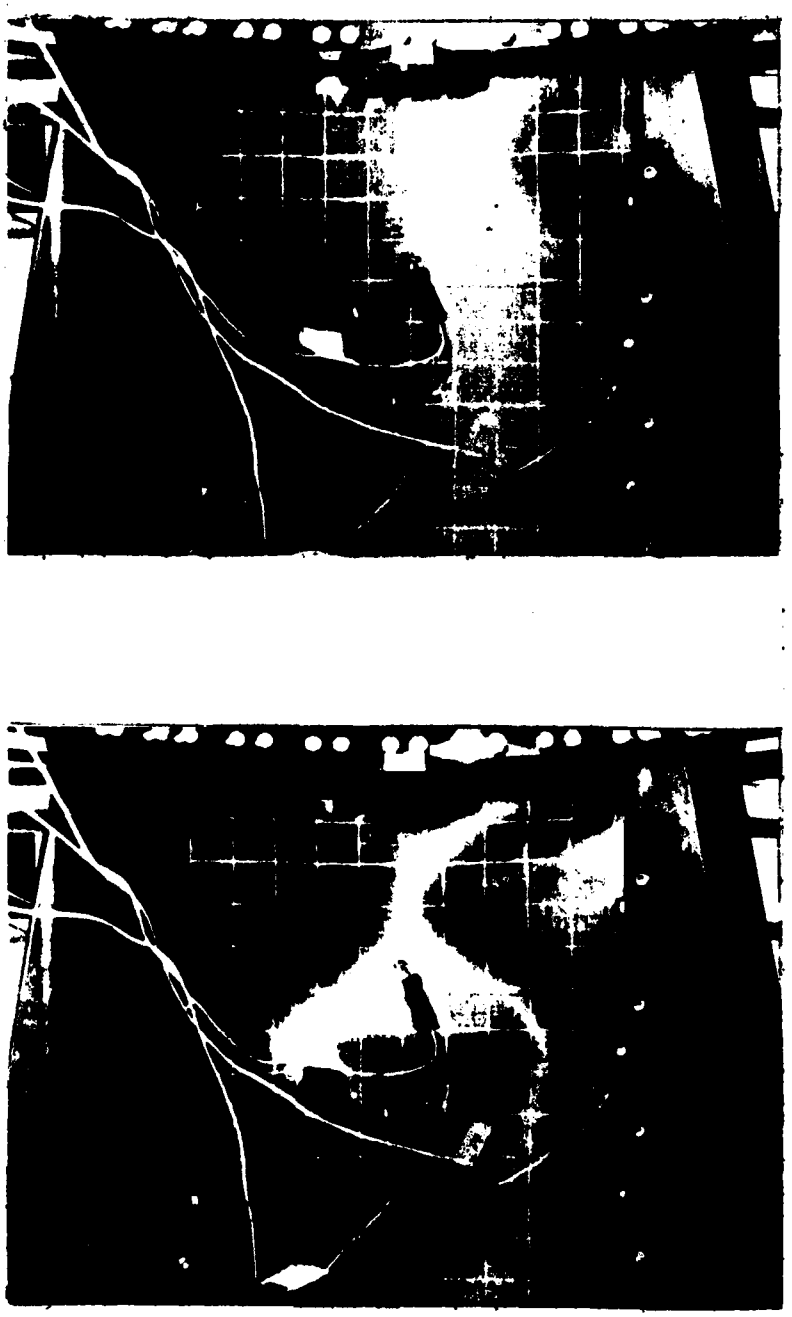

Figure 40 Buckling Progression for 4921 Panel

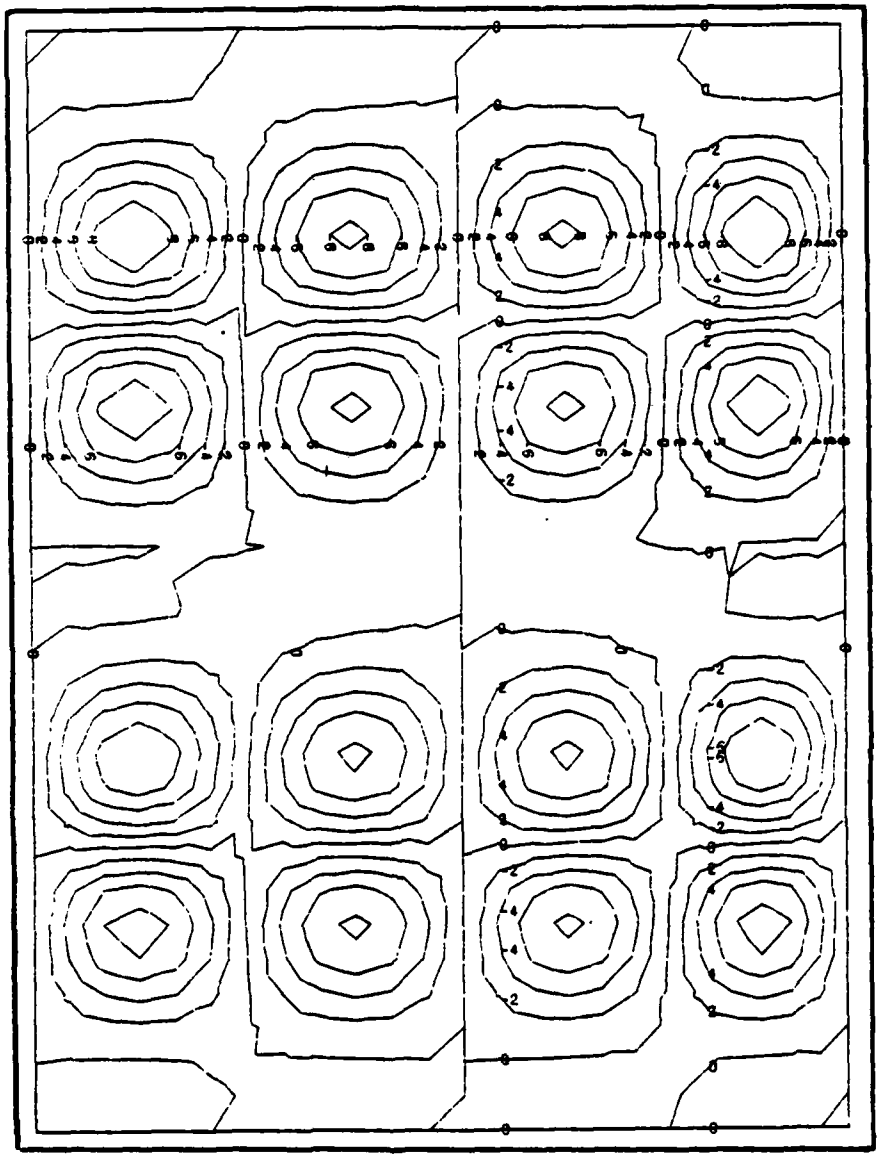

Figure 41 Analytical Buckling Pattern for 492 Panels

buckle can be explained by eccentricities in the test set-up since theory indicates that the first buckle should occur at the buckling load. In an attempt to explain this deviance from theory, the panel installation process was reexamined. Initially, all the panels were installed by entirely removing the left simple support. The right support was left in place with the set screws untightened to separate the knife edges. The panel was then slid in and clamped along the top and bottom curved edges. At this point the left support was reinstalled and set screws tightened on both left and right supports. The load was applied and the resulting pattern photographed.

A new installation procedure was followed and panels 1931, 1932, and 4931 were retested. This time both left and right supports were removed. This enabled the panels to be clamped along their top and bottom edges without interference, thus preventing a possible source of panel binding. The simple supports were then installed, knife edges meticulously centered, and the set screws finger tightened. This procedure was modified somewhat for the 1932 panel. The $\frac{1}{4}$ inch free space was placed at the bottom corners of this panel. This was accomplished by lifting the knife edges until they contacted the upper plate located at the top horizontal cross-head. The set screws were tightened just enough to keep the knife edges from sliding back down.

The new installation procedures produced significant results. It was observed that the final buckled configuration of both the 1931 and

4931 panels was the same as before the new installation procedures were implemented, see Fig's. 42 and 43. However, there was no buckling progression, indicating that the new installation procedure corrected the previous eccentricity problems. As per theory, both panels maintained their original shapes until the critical buckling load was reached; at which time they instantaneously snapped into their buckled configurations. It is important to note that the respective buckling loads associated with the two different installation procedures differed by only 3%. The most dramatic results were obtained when the ¼ inch free panel space was placed at the bottom. This configuration enabled the 1932 panel to buckle into the first symmetrical pattern observed in this thesis, see Fig. 44. It would appear that when simple supports are used, the panel's free space must be on the same end as the applied load. This allows for a more uniform stress distribution which results in buckling symmetry.

Ply Orientation/Aspect Ratio Effects

Given a specific ply orientation, Table II shows the analytical bifurcation loads decreased with increasing aspect ratio. This occurred experimentally with the $(90,\pm45,0)_s$ and $(\pm45)_{2s}$ panels. The $(90,0)_{2s}$ panels showed one deviation from this order with the 1-aspect ratio panels having the highest buckling load. Analytical values also

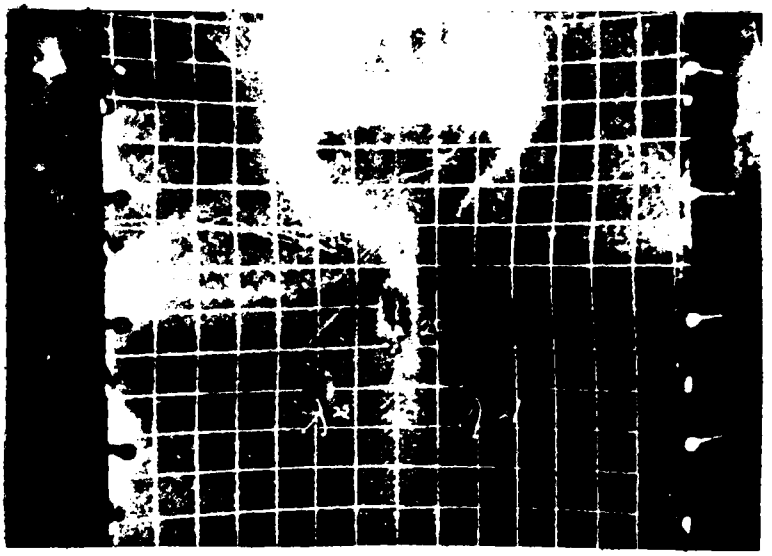

Figure 42 Buckling Pattern for Retested 1931 Panel

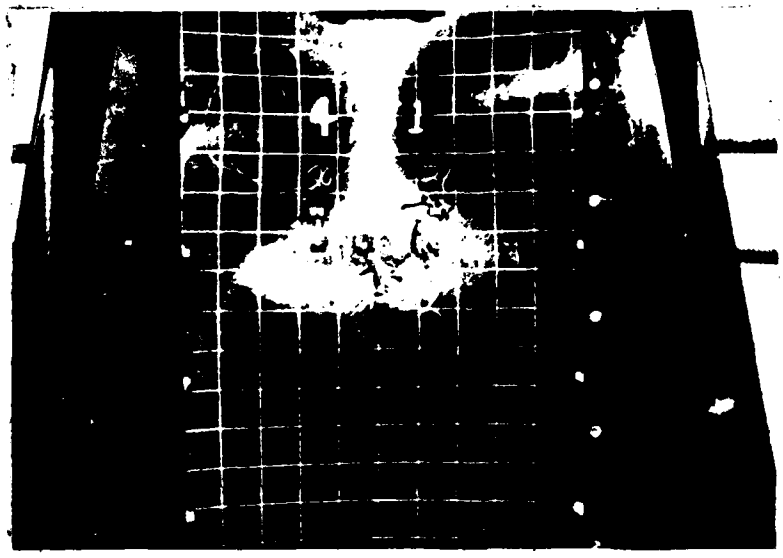

Figure 43 Buckling Pattern for Retested 4931 Panel

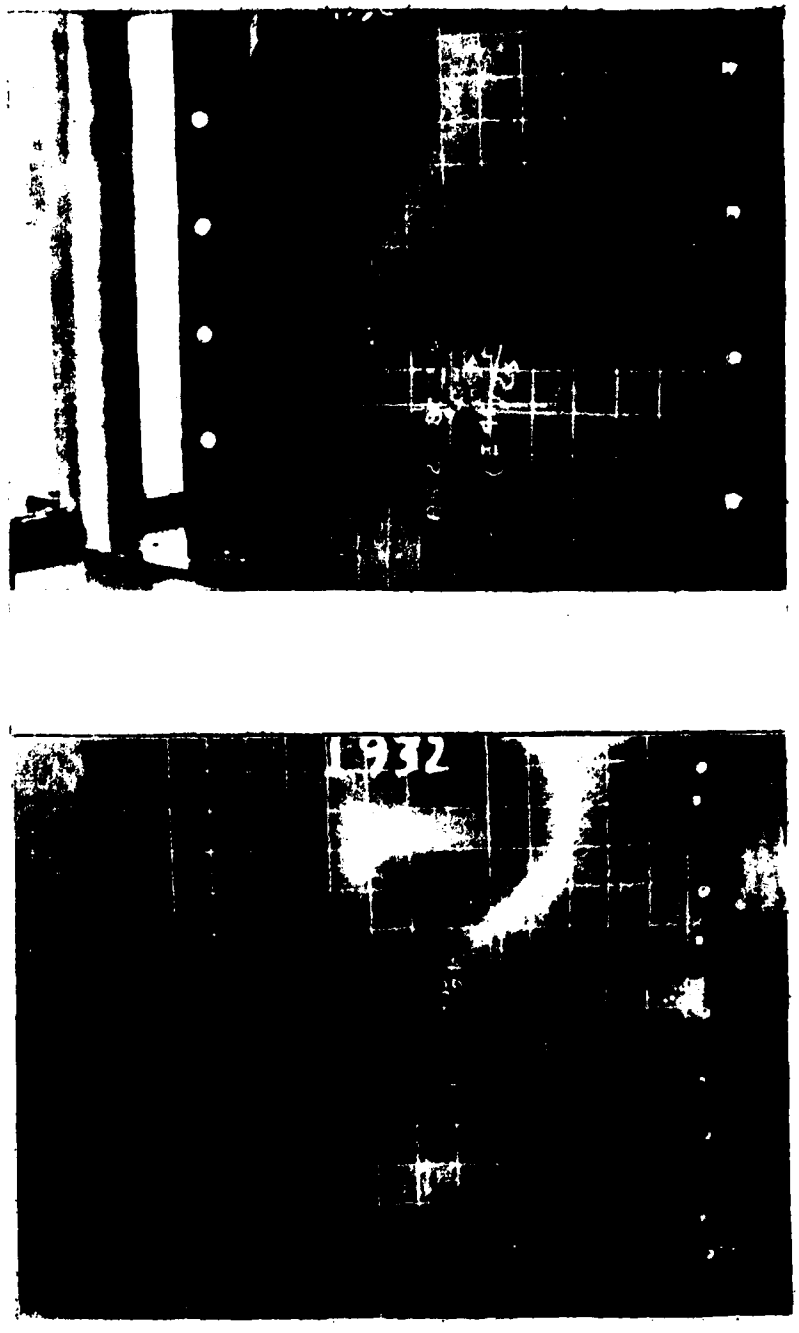

Figure 44 Symmetrical Buckling Pattern for Retested 1932 Panel

show that for a specific aspect ratio, the highest buckling load was associated with the $(90,\pm45,0)_s$ ply orientation followed by the $(\pm45)_{2s}$ and $(90,0)_{2s}$ orientations, respectively. Experimentally, this sequence was followed by only the ½ and 3/4 aspect ratio panels. (See Appendix C for the extentional and bending stiffness matrices for each ply orientation.)

It was determined that the aspect ratio had the greatest effect on a panel's buckling load, see Fig. 45. For the same ply orientation, the maximum increase in aspect ratio (½ to 2) produced over a 50% drop in buckling load both analytically and experimentally.

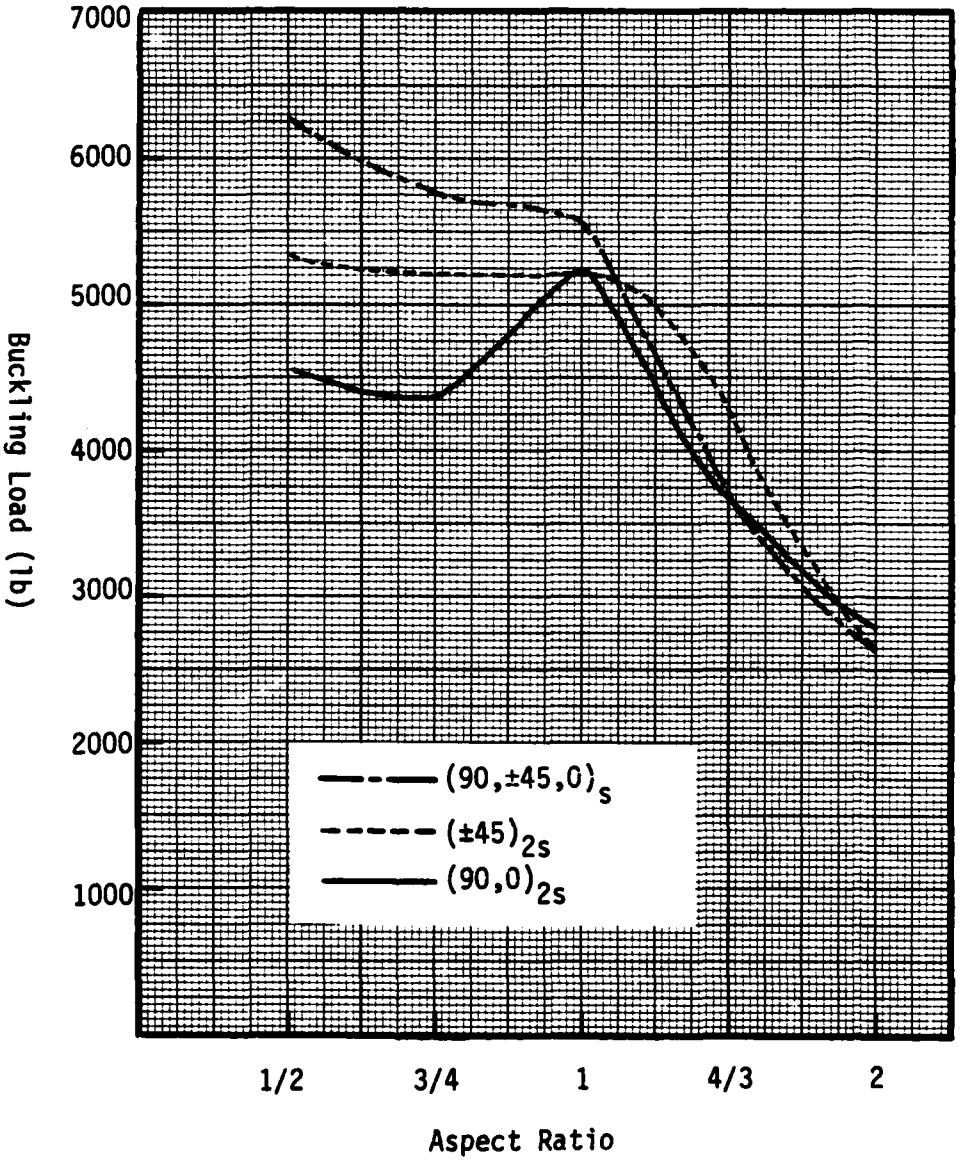

Figure 45 Experimental Buckling Load vs. Aspect Ratio

VI. CONCLUSIONS

Based on the analytical and experimental results the following conclusions can be made for composite cylindrical panels subjected to axial compressive loading.

1. Though the author sees imperfections as a very important contributor to bifurcation load, this thesis deals only with the linear bifurcation included within STAGSC-1. It can be seen that a linear analysis gives good results for the support device used.
2. The variance in knockdown factors precluded any general correlation between it and a panel's ply orientation and/or aspect ratio.
3. In a great majority of cases the observed buckling pattern did not exhibit the symmetry that would be expected by purely analytical means. It was found that the existing simple support device was the cause. Due to stress distribution considerations, the ½ inch free panel space must be on the same end as the applied load for a symmetrical buckling configuration to occur.
4. With any test device dealing with curved panels, the researcher should be particularly careful of the panel boundary restraints. A less than ideal installation procedure will cause panel eccentricities resulting in

initial buckles forming which do not correspond to the final buckling load of the panel.

5. The buckling pattern was more sensitive to boundary restraint irregularities than was the buckling load which remained essentially unchanged for a given panel.
6. It appears that the STAGSC-1 significantly overestimates the number of half-sine waves in the panels buckled configuration when compared to the number occurring experimentally.
7. The strain reversal and Southwell methods for determining buckling are generally inferior to the end-shortening method because strain reversal requires a prior knowledge of the buckling pattern and the Southwell method is particularly sensitive to panel eccentricities. However, from Table II, it can be seen that they provide a good check of the end-shortening method.
8. The amount of load a panel can carry is dependent upon its aspect ratio and ply orientation. It was found that for the boundary conditions used in this thesis, the aspect ratio had the greatest effect upon the buckling load followed by the ply orientation.
9. During the actual experimental loading of the panels, it was observed that the $(90,\pm45,0)_s$ and $(90,0)_{2s}$ panels

were more prone to breakage and splintering at the top corners than were the $(\pm 45)_{2s}$ panels. This appears to be due to the overall diagonal stiffening characteristic of the 45° oriented fibers.

10. As can be seen in Fig. 45, the difference in buckling loads associated with the three ply orientations used in this thesis generally decrease with increasing aspect ratio.

Bibliography

1. Hertz, et. al., "On the Track of Practical Forward Swept Wings," Astronautics and Aeronautics, 20: 28-41, January 1982.
2. Khot, N.S. and Venkayya, V.B., Effect of Fiber Orientation on Initial Postbuckling Behavior and Imperfection Sensitivity of Composite Cylindrical Shells, AFFDL-TR-70-125, WPAFB, Ohio: Air Force Flight Dynamics Laboratory, December 1970.
3. Booton, M. and Tennyson, R.C., "Buckling of Imperfect Anisotropic Circular Cylinders Under Combined Loading," AIAA Journal, 17: 278-287, March 1979.
4. Starnes, J.H., Jr., et. al., "Postbuckling Behavior of Selected Flat Stiffened Graphite-Epoxy Panels Loaded in Compression," Part 1: 464-478, May 1982.
5. Wilkens, D.J., "Compression Buckling Tests of Laminated Graphite-Epoxy Curved Panels," AIAA Paper No. 74-32. Presented at the AIAA 12th Aerospace Sciences Meeting, Washington, DC, January 30 - February 1, 1974.
6. Bauld, N.R., Jr., Experimental and Numerical Analysis of Axially Compressed Circular Cylindrical Fiber-Reinforced Panels with Various Boundary Conditions, AFWAL-TR-81-3158, WPAFB, Ohio: Air Force Wright Aeronautical Laboratories, August 1981.

Bibliography (Cont'd.)

7. Becker, M.L., Analytical/Experimental Investigation of the Instability of Composite Cylindrical Panels, Masters Thesis, WPAFB, Ohio: Air Force Institute of Technology, December 1979.

8. Arvin, G.H., et. al., Advanced Composites Design Guide, Vol I, Design, AFML-F33615-71-C-1362, WPAFB, Ohio: Air Force Materials Laboratory, January 1973.

9. Bushnell, D., Computerized Buckling Analysis of Shells, AFWAL-TR-81-3049, WPAFB, Ohio: Air Force Wright Aeronautical Laboratories, December 1981.

10. Brush, D.O. and Almroth, B.O., Buckling of Bars, Plates, and Shells, New York: McGraw-Hill, 1975.

11. Jones, R.M., Mechanics of Composite Materials, New York: McGraw-Hill, 1975.

12. Ashton, J.E., Halpin, J.C., and Petit, P.H., Primer on Composite Materials: Analysis, Conn: Technomic Publishing Co., 1969.

13. Bauld, N.R., Jr. and Satyamurthy, K., Collapse Load Analysis for Plates and Panels, AFFDL-TR-79-3038, WPAFB, Ohio: Air Force Flight Dynamics Laboratory, 1979.

14. Almroth, B.O., Brogan, F.A., and Stanley, G.M., Structural Analysis of General Shells, Volume II User Instructions for STAGSC-1, Lockheed Palo Alto Research Laboratory, California, January 1981.

15. Satyamurthy, K., Khot, N.S., and Bauld, N.R., Jr., "An Automated, Energy-Based, Finite-Difference Procedure for the Elastic Collapse of Rectangular Plates and Panels," Computers and Structures, II: 239-249, 1980.

16. Nelson, D.A., Buckling of Axially Compressed Stringer Stiffened Cylindrical Shells With and Without Cutouts, MS Thesis, WPAFB, Ohio: Air Force Institute of Technology, December 1977.

17. Almroth, B.O. and Brogan, F.A., Numerical Procedures for Analysis of Structural Shells, AFWAL-TR-3129, WPAFB, Ohio: Air Force Wright Aeronautical Laboratories, March 1981.

18. Snead, J.M., Moisture and Temperature Effects on the Instability of Cylindrical Composite Panels, MS Thesis, WPAFB, Ohio: Air Force Institute of Technology, December 1981.

19. Southwell, R.V., "On the Analysis of Experimental Observations in Problems of Elastic Stability," Proceedings of the Royal Society, A135: 601-616, London, 1932.

Appendix A

The Southwell Method

The Southwell Method [19] is a technique for obtaining the buckling load of a structure from experimental load deflection information. It has been used for the buckling of columns, beam columns, plates, and more recently, shells [5]. The method involves using the well established (free of test fixture slack) portion of an applied load (P) vs lateral deflection (δ) curve. Selected points are then normalized to obtain a plot of δ/p vs δ. A linear least squares fit of the points gives the slope of the line

$$\frac{\delta/P}{\delta} = \frac{1}{P} \tag{1A}$$

Inverting the slope gives the experimental buckling load, P. Figure 1-A shows P vs δ curve for the 3911 panel. The curve appears to be well established between 3000 and 5000 lbs. Data reduction was performed on 9 points in the above load range and is shown on Fig. 2-A. The Southwell buckling load was determined to be 5996.7 lbs.

AD-A124 664 ANALYTICAL/EXPERIMENTAL LINEAR BIFURCATION OF CURVED CYLINDRICAL COMPOSITE PANELS(U) AIR FORCE INST OF TECH WRIGHT-PATTERSON AFB OH SCHOOL OF ENGI.. J S HEBERT

2/2

UNCLASSIFIED DEC 82 AFIT/GAE/AA/82D-14 F/G 13/13 NL

END

FILMED

DTIC

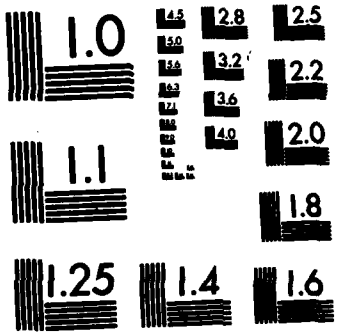

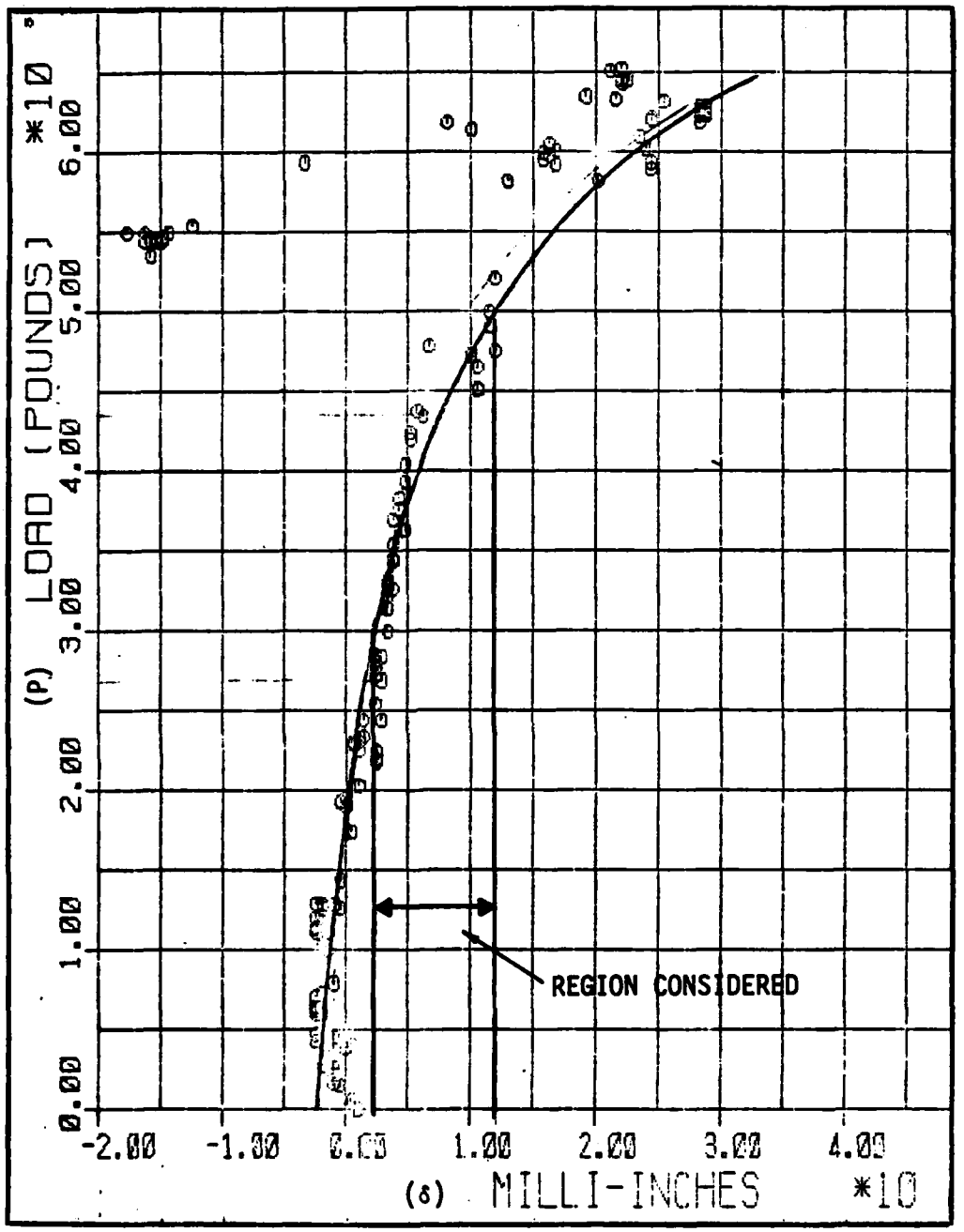

Figure 1-A Load vs. Radial Displacement for 3911 Panel

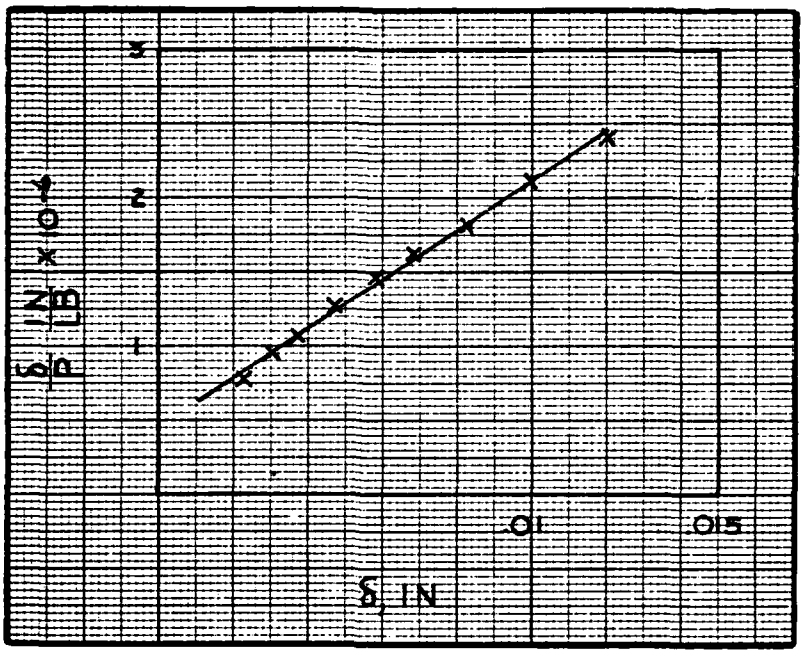

P	δ	$\delta/P \times 10^{-6}$
3000	.00229	.763
3250	.00308	.948
3500	.00375	1.07
3750	.00475	1.27
4000	.00583	1.46
4250	.00825	1.83
4750	.01000	2.11
5000	.01204	2.41

Slope Approx 1.667×10^{-4}/lb

Bifurcation Load $1/1.667 \times 10^{-4}$/lb = 5996.7 lbs

Figure 2-A Southwell Curve for 3911 Panel

Appendix B

STAGSC-1 Examples

Time/Space Limits The amount of computer time and space required by STAGSC-1 is dependent upon a panel's number of degrees of freedom. In this thesis, the 16x16 inch panels contained the most active degrees of freedom with 5985, while the 8x16 inch panels contained the least, 2913. The following maximum limits were found to be sufficient for all cases: CP Time = 1200 seconds, IO Time = 5000 seconds, and CM = 176,000 words. Figure 1-B shows the input data deck for the $(\pm 45)_{2s}$, 16"x16" panel. Figure 2-B shows the necessary control cards for the program. Consult reference [14] for further information.

```
CARD NUMBER      ********************************

     1                BIFURCATION ANALYSIS ON GR/EP
*****      C   (+- 45)2S SIMPLE SUPPORT 16X16
*****      C
*****      C   SIM45A
*****      C
     2                1,1,1,1,0                    $B1
     3                1,0                          $B2
     4                1,0,1,0                      $B3
     5                1.0                          $C1
     6                1,0,650,0,0                  $D2
     7                1,.290E03,0,0
     8                33,33                        $F1
     9                1,0                          $I1
    10                20.5E06,0.0212,
    11                0.75E06,0.0,0.0,
    12                1.3E06,0.0                   $I2
    13                1,1,8,0,0                    $K1
    14                1,.005,45.0                  $K2
    15                1,.005,-45.0
    16                1,.005,45.0
    17                1,.005,-45.0
    18                1,.005,-45.0
    19                1,.005,45.0
    20                1,.005,-45.0
    21                1,.005,45.0
    22                5,0                           $M1
    23                0.0,1[illegible].0,0.0,       $M2A
    24                83.621,12.0                  $M2A
    25                1,0                          $M5
    26                410
    27                0,0,0,0                      $P1
    28                100,000
    29                110,100                      $P2
    30                000,000
    31                110,100                      $P2
    32                1,0,0,0                      $Q1
    33                1,1,0                        $Q2
    34                1.0,2,1,1,0,0               $Q3
    35                1,1,1,0,0,1                    $R1
```

Figure 1-B Input Data Deck for the Linear Bifurcation Analysis of the 193 Panels

```
1.  HEB, T1200, I/O 5000, CM 176000.  D710554.
2.  ATTACH, PROCFIL, ID=A810171, SN=ASDAD.
3.  BEGIN, NOSFILE
4.  ATTACH, STAGS1, ID=D820138, MR=1.
5.  GET, SIM45A, ID=HEBERT.
6.  STAGS1, SIM45A.
7.  RETURN, STAGS1.
8.  ATTACH, STAGS2, ID=D820138.
9.  STAGS2, MR=1.
```

Figure 2-B Control Cards for the Linear Bifurcation Analysis of the 193 Panels

Appendix C

Extensional and Bending Stiffness Matrices

Extensional Stiffnesses

$$[A_{ij}] = \begin{bmatrix} A_{11} & A_{12} & A_{16} \\ A_{12} & A_{22} & A_{26} \\ A_{16} & A_{26} & A_{66} \end{bmatrix}$$

$(90,\pm45,0)_{2s}$

$$\begin{bmatrix} .35 & .11 & 0 \\ .11 & .35 & 0 \\ 0 & 0 & .12 \end{bmatrix} \times 10^6 \text{ lbf/in}$$

$(\pm45)_{2s}$

$$\begin{bmatrix} .26 & .20 & 0 \\ .20 & .26 & 0 \\ 0 & 0 & .21 \end{bmatrix} \times 10^6 \text{ lbf/in}$$

$(90,0)_{2s}$

Extension Stiffnesses (Cont'd.)

$$\begin{bmatrix} .44 & .02 & 0 \\ .02 & .44 & 0 \\ 0 & 0 & .03 \end{bmatrix} \times 10^6 \text{ lbf/in}$$

Bending Stiffnesses

$$[D_{ij}] = \begin{bmatrix} D_{11} & D_{12} & D_{16} \\ D_{12} & D_{22} & D_{26} \\ D_{16} & D_{26} & D_{66} \end{bmatrix}$$

$(90,\pm45,0)_s$

$$\begin{bmatrix} 19.72 & 12.11 & 4.82 \\ 12.11 & 77.59 & 4.82 \\ 4.82 & 4.82 & 13.77 \end{bmatrix} \text{ lbf-in}$$

$(\pm45)_{2s}$

$$\begin{bmatrix} 34.38 & 26.38 & 9.65 \\ 26.38 & 34.38 & 9.65 \\ 9.65 & 9.65 & 28.04 \end{bmatrix} \text{ lbf-in}$$

$(90,0)_{2s}$

Bending Stiffnesses (Cont'd.)

$$\begin{bmatrix} 39.12 & 2.34 & 0 \\ 2.34 & 77.72 & 0 \\ 0 & 0 & 4.00 \end{bmatrix} \text{ lbf-in}$$

Note: All coupling terms (B_{ij}) are zero since the three ply orientations are symmetric about their mid-surface.

As was previously mentioned, the buckling of shells is basically a bending problem. This obviously implies that the bending stiffness matrix is of primary importance in determining a shell's buckling load. Since an explicit equation for solving for the buckling load of a cylindrical shell was not available to the author, Eq. (1C), a buckling equation for a flat composite plate with an aspect ratio of 2 [10], was used to compare the relative sizes of the buckling loads associated with the 3 ply orientations used in this thesis.

$$\overline{N_x} = \frac{D_{11}}{4} + 2(D_{12} + 2D_{66}) + 4D_{22} \qquad (1C)$$

where $\overline{N_x}$ represents a force per unit length. Upon substituting the appropriate values for the D_{ij} into Eq. (1C), it was found that the $(90,\pm45,0)_{2s}$ had the largest buckling load followed by the $(90,0)_{2s}$

and $(\pm 45)_s$, respectively. This was not what occurred analytically nor in most cases experimentally, where it was found that the $(90,0)_{2s}$ orientation buckled at the lowest load. It is, therefore, evident that in shell analysis the extensional stiffness terms (A_{ij}) must also be included.

VITA

John S. Hebert was born on 29 May 1951 in Franklin, New Hampshire. He graduated from Franklin High School in 1969 and entered the University of New Hampshire where he received a Bachelor of Science Degree in Mechanical Engineering in 1974. He was commissioned in the USAF through the AF ROTC program at the University of New Hampshire and was assigned to Navigator training at Mather AFB, California. After serving 7 years as a navigator in KC and EC-135 aircraft, he was accepted into the graduate Aeronautical Engineering program at the AFIT School of Engineering in 1981.

Permanent address: 355 Victory Drive
Franklin, New Hampshire 03235

UNCLASSIFIED

SECURITY CLASSIFICATION OF THIS PAGE *(When Data Entered)*

REPORT DOCUMENTATION PAGE	READ INSTRUCTIONS BEFORE COMPLETING FORM
1. REPORT NUMBER: AFIT/GAE/AA/82D-14	2. GOVT ACCESSION NO.: AD-A124664
	3. RECIPIENT'S CATALOG NUMBER
4. TITLE *(and Subtitle)*: Analytical/Experimental Linear Bifurcation of Curved Cylindrical Composite Panels	5. TYPE OF REPORT & PERIOD COVERED: MS Thesis
	6. PERFORMING ORG. REPORT NUMBER
7. AUTHOR(s): John S. Hebert, Capt USAF	8. CONTRACT OR GRANT NUMBER(s)
9. PERFORMING ORGANIZATION NAME AND ADDRESS: Air Force Institute of Technology (AFIT/EN) Wright-Patterson AFB, Ohio 45433	10. PROGRAM ELEMENT, PROJECT, TASK AREA & WORK UNIT NUMBERS
11. CONTROLLING OFFICE NAME AND ADDRESS: Air Force Institute of Technology (AFIT/EN) Wright-Patterson AFB, Ohio 45433	12. REPORT DATE: December 1982
	13. NUMBER OF PAGES: 104
14. MONITORING AGENCY NAME & ADDRESS *(if different from Controlling Office)*	15. SECURITY CLASS. *(of this report)*: Unclassified
	15a. DECLASSIFICATION/DOWNGRADING SCHEDULE

16. DISTRIBUTION STATEMENT *(of this Report)*

Approved for public release; distribution unlimited.

17. DISTRIBUTION STATEMENT *(of the abstract entered in Block 20, if different from Report)*

18. SUPPLEMENTARY NOTES

Approved for public release: IAW AFR

LYNN E. WOLAVER
Dean for Research and Professional Development
Air Force Institute of Technology (AIC)
Wright-Patterson AFB OH 45433

6 JAN 1983

19. KEY WORDS *(Continue on reverse side if necessary and identify by block number)*

Bifurcation Analysis
Buckling
Cylindrical Composite Panels
Knockdown Factors
Boundary Conditions
Aspect Ratio

20. ABSTRACT *(Continue on reverse side if necessary and identify by block number)*

The Buckling Loads of 8-ply unstiffened (Graphite-Epoxy) cylindrical panels were determined experimentally. The results were compared to the linear bifurcation loads as determined by the STAGSC-1 Computer Code. The analysis included three different ply orientations, five different aspect ratios, and one set of boundary conditions; clamped along the top and bottom curved edges and simply supported along the vertical edges.

DD FORM 1 JAN 73 1473 EDITION OF 1 NOV 65 IS OBSOLETE

UNCLASSIFIED

SECURITY CLASSIFICATION OF THIS PAGE *(When Data Entered)*

END

FILMED

3-83

DTIC